Classical statistical mechanics of the sine-Gordon and ϕ^4 chain. II. Dynamic properties

T. Schneider and E. Stoll
IBM Zurich Research Laboratory, 8803 Rüschlikon, Switzerland
(Received 7 July 1980)

We present and discuss the classical statistical mechanics of the dynamic properties associated with a discretized sine-Gordon and ϕ^4 system by using the molecular-dynamics technique. To calibrate the interpretation, various approximate expressions for the dynamic form factors of interest are derived on the basis of an interacting phonon gas and an ideal kink gas. On this basis, kink, phonon, and second-sound excitation branches are identified. The occurrence of the kink excitation branch turns out to be restricted to small wave numbers and frequencies and to low temperatures. Evidence for breather features, distinct from anharmonic contributions, is also given.

I. INTRODUCTION

In a previous paper,[1] we studied the static properties associated with a discretized sine-Gordon (sG) and ϕ^4 system, to clarify the relevance of the associated soliton features in thermodynamic properties and static form factors, to identify soliton-sensitive properties, and to test the validity of approximate treatments. The present work extends this study to the statistical mechanics of dynamic properties. We shall concentrate on molecular-dynamics (MD) results for dynamic form factors which are the most revealing properties to unravel the excitation spectrum. Because of the lack of a firmly based theory for the classical mechanics of dynamic properties in these systems,[2] the present work provides a solid basis for a confrontation with approximate treatments.[3–7]

The following results are obtained:

(i) Confirming our previous results,[8–10] in both the sG and ϕ^4 chains, we find a kink excitation branch, exhausting the spectrum of the displacement dynamic form factor for small wave numbers and low temperatures. In the sG case, the MD results agree rather well with the predictions resulting from an ideal kink (soliton) gas approximation, exhibiting pronounced relativistic effects. The importance of a thermal kink energy renormalization turns out to be crucial. For the ϕ^4 chain, the agreement is less quantitative and becomes even worse on the inclusion of thermal renormalization.

(ii) An ideal kink-gas approximation is formulated to estimate dynamic form factors at low temperatures. Consistency with the corresponding exact static form factors, as derived with the aid of the transfer integral method, requires a particular decomposition of the displacement field in terms of kinks. The decomposition, consistent with this requirement, turns out to be fundamentally different in the sG and ϕ^4 systems, and reflects the fact that in the ϕ^4 case, kink and antikinks can occur pairwise only. As mentioned above, the results agree quite well with MD.

(iii) To substantiate the identification of the kink excitation branch, we also present snapshots of the displacement patterns and the time evolution of the signals of a π and sign detector. On this basis, the existence of thermalized kinks and large-amplitude breatherlike soliton features is clearly demonstrated. These patterns also reveal the creation and annihilation channels, and illustrate the fundamental difference in the motion of thermalized kinks in the sG and ϕ^4 chains. In the sG case, the relativistic effects are clearly seen, while in the ϕ^4 chain, the kink motion turns out to be random-walk-like.

(iv) For larger wave numbers and low temperatures, or for intermediate temperatures and all wave numbers, the dynamic displacement form factor is found to be dominated by an optic-phonon branch. These results are explained in terms of a high- and low-frequency approximation, appropriate for an interacting phonon gas.

(v) The high-temperature behaviors of the two systems turn out to be fundamentally different. In the limit $T \to \infty$, the sG chain tends to a weakly interacting phonon gas, because the nonlinear single-site potential becomes irrelevant. In view of this, it can be understood that the dynamic form factor associated with the energy fluctuations exhibits a well-defined second-sound resonance, not only at low and intermediate but also at high temperatures. The ϕ^4 chain, however, in this limit becomes equivalent to a set of independent quartic oscillators. This fact explains the absence of kink features, and less well-defined second sound in the MD results for high temperatures.

(vi) The MD results for dynamic form factors, expected to be kink insensitive, are partially explained in terms of anharmonic perturbation theory and

breatherlike features.

(vii) The critical slowing down in the ϕ^4 chain, associated with the displacement fluctuations and $q=0$, is elucidated in terms of the kink excitation branch. The softening of the gap of the optic-phonon branch turns out to be incomplete.

(viii) Exact results for the frequency moments and relations between dynamic form factors are derived.

In Sec. II, we summarize the definition of the models and of the associated quantities of interest. Exact results for the frequency moments and relations between dynamic form factors are derived in Sec. III, while in Sec. IV, we summarize approximate calculations of the dynamic form factors of interest to calibrate the discussion of the MD results. They include: a high- and low-frequency approximation, appropriate for an interacting phonon gas, heat diffusion, and second sound, two-phonon approximation for kink-insensitive dynamic form factors, valid at low temperatures, high-temperature approximations, an ideal kink-gas approximation. In Sec. VI, we present and discuss some MD results of the sG chain, while Sec. VII is devoted to the ϕ^4 results.

We trust that these results have opened a door on nonlinear, solitonlike phenomena, which are absent in nearly linear systems.

II. MODELS AND DEFINITIONS

In this section, we briefly summarize the definition of the models and the associated quantities of interest. For a more detailed discussion, we refer to Ref. 1.

The sG and ϕ^4 chains belong to the general class of Hamiltonians of the form

$$\mathcal{H}=\sum_l Da\left[\frac{\dot{y}_l^2}{2}+\omega_0^2 V(y_l)+\frac{c_0^2}{2a^2}(y_{l+1}-y_l)^2\right] , \quad (1)$$

where y_l is a scalar dimensionless displacment on a one-dimensional reference lattice of points (labeled by l) with lattice constant a. The system can be viewed as an elastic chain, subjected to a superposition of single-site potentials $V(y_l)$. A characteristic velocity is c_0, and ω_0 is a characteristic frequency of the system. The energy scale is set by D and is given by

$$D=Ma \ . \quad (2)$$

The single-site potentials considered here are given by

$$\omega_0^2 V(y)=\omega_0^2\frac{b}{4}\left[y^2-\frac{1}{b}\right]^2-\frac{\omega_0^2}{4b}$$

$$=-\Delta\frac{y^2}{2}+\frac{B}{4}y^4, \quad \phi^4 \text{ chain} , \quad (3)$$

$$V(y)=1-\cos y, \quad \text{sG chain} , \quad (4)$$

where

$$\Delta=\omega_0^2, \quad B=b\omega_0^2 \ . \quad (5)$$

In the continuum limit, Hamiltonian (1) reduces to

$$\mathcal{H}=Da\int dy\left[\frac{1}{2}\dot{\phi}^2+\frac{c_0^2}{2}\phi_y^2+\omega_0^2 V(\phi)\right] , \quad (6)$$

with the associated equation of motion,

$$\ddot{\phi}-c_0^2\phi_{yy}+\omega_0^2\frac{dV}{d\phi}=0 \ . \quad (7)$$

The kink solitary wave solutions, as obtained from Eqs. (3)–(7), and the associated kink energies,[11]

$$E_k=\gamma E_k^0, \quad \gamma=\left[1-\frac{v^2}{c_0^2}\right]^{-1/2} , \quad (8)$$

are listed in Table I. The parameter d is defined by

$$d=\frac{c_0}{\omega_0} , \quad (9)$$

and ξ denotes

$$\xi=y-vt , \quad (10)$$

where v is the kink velocity. The "relativistic" dependence of the kink energy and the kink solutions reflects the Lorentz invariance of Hamiltonian (6).[11]

III. EXACT RESULTS: FREQUENCY MOMENTS AND RELATIONS BETWEEN DYNAMIC FORM FACTORS

In this section, we derive exact results including frequency moments of and relations between dynamic form factors. These results represent a useful

TABLE I. Kink solution ϕ_k and kink rest energy E_k^0 for the sG and ϕ^4 system. (From T. Schneider and E. Stoll, Springer Series in Solid-State Sciences 23, 1981, p.76.)

V	$1-\cos\phi$	$\frac{b}{4}\left[\phi^2-\frac{1}{b}\right]^2-\frac{1}{4b}$
ϕ_k	$4\tan^{-1}\exp\pm\frac{\gamma\xi}{d}$	$\frac{1}{\sqrt{b}}\tanh\pm\frac{\gamma\xi}{d}\left[\frac{b}{2}\right]^{1/2}$
E_k^0	$8D\omega_0 c_0$	$2\frac{\sqrt{2}}{3}D\omega_0 c_0\frac{1}{b}$

basis to test and interpret approximate treatments and numerical results. Assuming the establishment of thermal equilibrium, dynamic form factors are the most revealing properties to unravel the excitation spectrum. They are defined by

$$S_{AA}(q,\omega)=\int_{-\infty}^{+\infty} dt[\exp(-i\omega t)]S_{AA}(q,t) \ , \quad (11)$$

where

$$S_{AA}(q,t)=\langle A(q,t)A(-q,0)\rangle \ , \quad (12)$$

$$A(q,t)=\frac{1}{\sqrt{N}}\sum_l(\exp iqal)\delta A_l \ ,$$
$$\delta A_l=A_l-\langle A_l\rangle \ . \quad (13)$$

A_l is a dynamic variable related to the basic variables entering the Hamiltonian [Eq. (1)]. The wave number is q, the frequency ω, and l labels the sites of the rigid reference lattice with lattice constant a. Next, we derive various expressions for the frequency moments of $S_{AA}(q,\omega)$ and finally, determine relations between some dynamic form factors.

A. Frequency moments

To derive useful expressions for the frequency moments

$$\left.\frac{d^n}{dt^n}S_{AA}(q,t)\right|_{t=0}=(i)^n\int_{-\infty}^{+\infty}\frac{d\omega}{2\pi}\omega^n S_{AA}(q,\omega) \ , \quad (14)$$

we summarize some properties of $S_{AA}(q,t)$. For a classical system evolving according to Newton's equations, we have

$$S_{AA}(q,t)=S_{AA}(q,-t) \ , \quad (15)$$

$S_{AA}(q,t)$ being analytic for $t\to 0$. It then follows that

$$\left.\frac{d^n}{dt^n}S_{AA}(q,t)\right|_{t=0}=0 \ , \quad (16)$$

if n is odd. Another important property follows from the translational invariance of the correlation functions, namely,

$$\langle A(t)B(t+\tau)\rangle=\langle A(0)B(\tau)\rangle \ , \quad (17)$$

so that

$$\frac{d}{dt}\langle A(t)B(t+\tau)\rangle=0 \ , \quad (18)$$

$$\langle\dot{A}(0)B(0)\rangle=\langle A(0)\dot{B}(0)\rangle \ ,$$
$$-\langle\ddot{A}(0)B(0)\rangle=\langle\dot{A}(0)\dot{B}(0)\rangle \ , \quad (19)$$

where

$$\left.\frac{dA(t)}{dt}\right|_{t=0}=\dot{A}(0) \ . \quad (20)$$

Using the properties listed in Eqs. (16) and (19), it is now easily seen that

$$S_{AA}(q)=S_{AA}^{(0)}(q)=S_{AA}(q,t=0)$$
$$=\int_{-\infty}^{+\infty}\frac{d\omega}{2\pi}S_{AA}(q,\omega) \ , \quad (21)$$

$$S_{AA}^{(2)}(q)=-\ddot{S}_{AA}(q,t=0)=\langle\dot{A}(q)\dot{A}(-q)\rangle$$
$$=\int_{-\infty}^{+\infty}\frac{d\omega}{2\pi}\omega^2 S_{AA}(q,\omega) \ , \quad (22)$$

$$S_{AA}^{(4)}(q)=\dddot{S}_{AA}(q,t=0)=\langle\ddot{A}(q)\ddot{A}(-q)\rangle$$
$$=\int_{-\infty}^{+\infty}\frac{d\omega}{2\pi}\omega^4 S_{AA}(q,\omega) \ . \quad (23)$$

TABLE II. Definition of some dynamic variables for the sG chain and notation of the associated diagonal dynamic form factors.

Variable	Dynamic form factor
$y(q)=\frac{1}{\sqrt{N}}\sum_l(\exp iqal)y_l$	$S_{yy}(q,\omega)$
$s(q)=\frac{1}{\sqrt{N}}\sum_l(\exp iqal)\sin y_l$	$S_{ss}(q,\omega)$
$c(q)=\frac{1}{\sqrt{N}}\sum_l(\exp iqal)(\cos y_l-\langle\ \rangle)$	$S_{cc}(q,\omega)$
$H(q)=\frac{1}{\sqrt{N}}\sum_l(\exp iqal)\left[Da\left(\frac{\dot{y}_l^2}{2}+\omega_0^2V(y_l)+\frac{c_0^2}{4a^2}[(y_{l+1}-y_l)^2+(y_l-y_{l+1})^2]\right)\right]$	$S_{HH}(q,\omega)$

TABLE III. Frequency moments $S_{AA}^{(n)}(q) = \int \omega^n (d\omega/2\pi) S_{AA}(q,\omega)$ for the sG chain.

$S_{yy}^{(2)}(q)$	$\frac{k_B T}{Da}$
$\frac{S_{yy}^{(4)}(q)}{S_{yy}^{(2)}(q)}$	$\omega_0^2 \langle \cos y_l \rangle + \frac{2c_0^2}{a^2}(1-\cos qa) = \omega_A^2$
$S_{ss}(q=0)$	$\frac{k_B T}{Da\,\omega_0^2} \langle \cos y_l \rangle$
$S_{ss}^{(2)}(q)$	$\frac{k_B T}{Da} \langle (\cos y_l)^2 \rangle$
$S_{cc}^{(2)}(q)$	$\frac{k_B T}{Da} \langle (\sin y_l)^2 \rangle$
$S_{HH}^{(2)}(q)$	$\left[\frac{Dac_0^2}{a^2}\right]^2 \frac{k_B T}{Da} \frac{1}{N} \sum_{q'} \langle \lvert y(q') \rvert^2 \rangle [\cos q' - \cos(q-q') + (\cos q) - 1]^2$

The extension to higher-frequency moments is straightforward.

To obtain explicit expressions for these frequency moments, we use the equations of motion. Specifically, we treat the sG chain only, because the derivation is quite analogous for the ϕ^4 chain. The classical equation of motion of the sG chain is, according to Eqs. (1) and (4),

$$-\ddot{y}_l = \omega_0^2 \sin y_l + \frac{c_0^2}{a^2}(2y_l + y_{l+1} - y_{l-1}) \tag{24}$$

or

$$-\ddot{y}(q) = \omega_0^2 s(q) + 2\frac{c_0^2}{a^2}(1-\cos qa)\, y(q) \ , \tag{25}$$

where, according to Eq. (13),

$$y(q) = \frac{1}{\sqrt{N}} \sum_l (\exp iqal) y_l \ , \tag{26}$$

$$s(q) = \frac{1}{\sqrt{N}} \sum_l (\exp iqal) \sin y_l \ . \tag{27}$$

A list of variables of interest are given in Table II. Noting that

$$\langle \dot{y}_i \dot{y}_j \rangle = \left[\frac{2\pi}{\beta Da}\right]^{N/2} \int_{-\infty}^{+\infty} \dot{y}_i \dot{y}_j \prod_{i=1}^{N} \exp\left[-\frac{\beta Da \dot{y}_i^2}{2}\right] d\dot{y}_i$$

$$= \frac{k_B T}{Da} \delta_{ij} \ , \tag{28}$$

TABLE IV. Definition of some variables for the ϕ^4 chain and notation of the associated diagonal dynamic form factors.

Variable	Dynamic form factor
$y(q) = \frac{1}{\sqrt{N}} \sum_l \exp iqal\, y_l$	$S_{yy}(q,\omega)$
$y^2(q) = \frac{1}{\sqrt{N}} \sum_l \exp iqal (y_l^2 - \langle y_l^2 \rangle)$	$S_{y^2y^2}(q,\omega)$
$H(q) = \frac{1}{\sqrt{N}} \sum_l (\exp iqal) Da \left[\frac{\dot{y}_l^2}{2} + \omega_0^2 \frac{b}{4}\left(y_l^2 - \frac{1}{b}\right)^2 - \frac{\omega_0^2}{4b} + \frac{c_0^2}{4a^2}[(y_{l+1}-y_l)^2 + (y_l - y_{l-1})^2]\right]$	$S_{HH}(q,\omega)$
$y^3 = \frac{1}{\sqrt{N}} \sum_l \exp iqal\, y_l^3$	$S_{y^3y^3}(q,\omega)$

TABLE V. Frequency moments $S_{AA}^{(n)}(q)=\int (d\omega/2\pi)\omega^n S_{AA}(q,\omega)$ for the ϕ^4 chain.

$S_{yy}^{(2)}(q)$	$\frac{k_B T}{Da}$
$\frac{S_{yy}^{(4)}(q)}{S_{yy}^{(2)}(q)}$	$-\omega_0^2+3b\omega_0^2\langle y_l^2\rangle+\frac{2c_0^2}{a^2}(1-\cos qa)=-\Delta+3B\langle y_l^2\rangle+\frac{2c_0^2}{a^2}(1-\cos qa)=\omega_A^2$
$S_{HH}^{(2)}(q)$	$\left[\frac{Dac_0^2}{a^2}\right]^2\frac{k_B T}{Da}\frac{1}{N}\sum_{q'}\langle\lvert y(q')\rvert^2\rangle[\cos q'-\cos(q-q')+(\cos q)-1]^2$

we obtain from Eqs. (22), (25), and (28)

$$
\begin{aligned}
-\langle\ddot{y}(q)y(-q)\rangle &= \langle\dot{y}(q)\dot{y}(-q)\rangle \\
&= S_{yy}^{(2)}(q)=\frac{k_B T}{Da} \\
&= \omega_0^2\langle s(q)y(-q)\rangle \\
&\quad+\frac{2c_0^2}{a^2}(1-\cos qa)\langle y(q)y(-q)\rangle \\
&= \omega_0^2 S_{sy}(q)+\frac{2c_0^2}{a^2}(1-\cos qa)S_{yy}(q) \ .
\end{aligned}
\tag{29}
$$

This result reveals that the second frequency moment does not depend on the details of the interaction and of the single-site potential. Nevertheless, Eq. (29) provides a useful relation between the static form factors $S_{yy}(q)$ and $S_{sy}(q)$.

To derive an expression for the fourth frequency moment, we consider the first time derivative of the equation of motion (25),

$$
\begin{aligned}
-\dddot{y}(q) &= \omega_0^2\dot{S}(q)+\frac{2c_0^2}{a^2}(1-\cos qa)\dot{y}(q) \\
&= \omega_0^2\frac{1}{\sqrt{N}}\sum_l e^{iqal}\cos y_l\dot{y}_l \\
&\quad+\frac{2c_0^2}{a^2}(1-\cos qa)\dot{y}(q) \ .
\end{aligned}
\tag{30}
$$

It then follows from Eqs. (23) and (28),

$$
\begin{aligned}
-\langle\ddot{y}(q)\dddot{y}(-q)\rangle &= \langle\ddot{y}(q)\ddot{y}(-q)\rangle=S_{yy}^{(4)}(q) \\
&= \frac{k_B T}{Da}\left[\omega_0^2\langle\cos y_l\rangle+\frac{2c_0^2}{a^2}(1-\cos qa)\right] \ ,
\end{aligned}
\tag{31}
$$

revealing that the fourth frequency moment depends on the interaction and the single-site potential. This is also true for the higher-frequency moments.

This approach also yields frequency moments of $S_{ss}(q,\omega)$ and $S_{cc}(q,\omega)$ as summarized in Table III.

In the ϕ^4 chain, we shall concentrate on the variables listed in Table IV. Some frequency moments are given in Table V.

B. Relations between dynamic form factors

Since the equation of motion (25) relates the time evolution of $y(q,t)$ and $s(q,t)$, the dynamic form factors $S_{yy}(q,\omega)$ and $S_{ss}(q,\omega)$ will not be independent. The relationship might be obtained as follows: From Eq. (25),

$$
\begin{aligned}
-\langle\ddot{y}(q,t)s(q,0)\rangle &= \omega_0^2\langle s(q,t)s(-q,0)\rangle \\
&\quad+\frac{2c_0^2}{a^2}(1-\cos qa)\langle y(q,t)s(q,0)\rangle
\end{aligned}
\tag{32}
$$

or

$$
-\ddot{S}_{ys}(q,t)=\omega_0^2 S_{ss}(q,t)+\frac{2c_0^2}{a^2}(1-\cos qa)S_{ys}(q,t) \ . \tag{33}
$$

On Fourier transforming, we find

$$
\omega_0^2 S_{ss}(q,\omega)=\left[\omega^2-\frac{2c_0^2}{a^2}(1-\cos qa)\right]S_{ys}(q,\omega) \ . \tag{34}
$$

Using the equation of motion in the form

$$
\omega_0^2 s(q,t)=\ddot{y}(q,t)+2\frac{c_0^2}{a^2}(1-\cos qa)y(q,t) \ , \tag{35}
$$

it then follows

$$
\begin{aligned}
\omega_0^4 S_{ss}(q,t) &= \ddddot{S}_{yy}(q,t)+4\frac{c_0^2}{a^2}(1-\cos qa)\ddot{S}_{yy}(q,t) \\
&\quad+\left[2\frac{c_0^2}{a^2}(1-\cos qa)\right]^2 S_{yy}(q,t) \ ,
\end{aligned}
\tag{36}
$$

TABLE VI. Relations between dynamic form factors.

sG chain

$$\omega_0^4 S_{ss}(q,\omega) = S_{yy}(q,\omega)\left[\omega^2 - \frac{2c_0^2}{a^2}(1-\cos qa)\right]^2$$

$$\omega_0^2 S_{ss}(q,\omega) = S_{ys}(q,\omega)\left[\omega^2 - \frac{2c_0^2}{a^2}(1-\cos qa)\right]$$

$$S_{yy}(q,\omega)S_{ss}(q,\omega) = [S_{ys}(q,\omega)]^2$$

ϕ^4 chain

$$B^2 S_{y^3y^3}(q,\omega) = S_{yy}(q,\omega)\left[\omega^2 - \left[\Delta - \frac{2c_0^2}{a^2}(1-\cos qa)\right]\right]^2$$

$$B S_{y^3y^3}(q,\omega) = S_{yy^3}(q,\omega)\left[\omega^2 - \left[\Delta - \frac{2c_0^2}{a^2}(1-\cos qa)\right]\right]$$

$$S_{yy}(q,\omega)S_{y^3y^3}(q,\omega) = [S_{yy^3}(q,\omega)]^2$$

and on Fourier transforming,

$$\omega_0^4 S_{ss}(q,\omega) = S_{yy}(q,\omega)\left[\omega^2 - \frac{2c_0^2}{a^2}(1-\cos qa)\right]^2 . \quad (37)$$

Combining Eqs. (34) and (37) it is seen that

$$S_{yy}(q,\omega)S_{ss}(q,\omega) = [S_{ys}(q,\omega)]^2 , \quad (38)$$

which, in general, only holds as an inequality. These results are summarized in Table VI, where we also list relations for the ϕ^4 chain, following from the corresponding prescriptions outlined above. These relations are obviously very useful to test approximate and numerical results for the dynamical form factors.[12]

IV. APPROXIMATE TREATMENTS OF DYNAMIC FORM FACTORS

To examine and interpret the resonance structure of dynamic form factors, it is useful to derive approximate expressions, including dispersion laws for the peak positions in $S_{AA}(q,\omega)$. Moreover, these derivations may also shed light onto the physical origin of the possible excitation branches. In the formulation of a strategy, it is necessary to be consistent with the behavior of the static properties, discussed in detail in Ref. 1. The essential features might be summarized as follows: At high temperatures ($k_B T > E_k^0$), the kinks become irrelevant. In fact, the sG chain tends to a harmonic system, while the ϕ^4 chain becomes equivalent to a set of independent quartic oscillators. At low temperatures ($k_B T << E_k^0$), the kink-insensitive properties are well described by anharmonic perturbation theory. For kink-sensitive properties, kink effects are restricted to small q values, and on physical grounds also to small ω values only. In the intermediate-temperature regime, these approaches fail, because they are valid only in the corresponding temperature limits. From the dynamic point of view, one has also to consider the occurrence of the hydrodynamic mode, associated with energy conservation, namely, heat diffusion or second sound.

Taking these constraints into account, we shall develop high-frequency approximations for the kink-sensitive $S_{yy}(q,\omega)$, by neglecting the kink contribution occurring at small q and ω values. The kink effects will be taken into account in terms of the soliton-gas approach. For low temperatures and kink-insensitive dynamic form factors, we use anharmonic perturbation theory. In the sG chain, this approximation is also applied to the high-temperature behavior, in terms of a high-temperature phonon basis.

A. High-frequency approximations

When one uses the resolvent representation of the retarded Green's function,[13,14] the Green's-function matrix $G_{AA}^{+}(z)$ for n-dynamic variables,

$$A = (A_1, \ldots, A_n) \quad (39)$$

can be written as

$$G_{AA}^{+}(z) = -\beta a\,(za - \Omega + iF)^{-1}(-\Omega + iF) , \quad (40)$$

where

$$\Omega_{ij} = -i\langle \dot{A}_i | A_j \rangle = -i\langle \dot{A}(q) A(-q) \rangle , \quad (41)$$

$$a_{ij} = \langle A_i | A_j \rangle = \langle A(q) A(-q) \rangle , \quad (42)$$

$$F_{ij} = \left\langle \dot{A}_i\, Q \frac{i}{z - QLQ} Q\, \dot{A}_j \right\rangle , \quad (43)$$

$$Q = 1 - P , \quad (44)$$

$$P = \sum_{i,j} |A_i\rangle (a^{-1})_{ij} \langle A_j| . \quad (45)$$

The Green's functions introduced here are related to the dynamic form factors [Eq. (11)] by

$$\chi_{AB}(\omega) = -\lim_{\epsilon \to 0} G_{AB}(z = \omega + i\epsilon) , \quad (46)$$

$$\chi''_{AB}(\omega) = \pi\beta\omega S_{AB}(\omega) , \quad (47)$$

χ'' being the imaginary part of the susceptibility χ.

At high frequencies, in $S_{yy}(q,\omega)$ we expect resonances due to an optic-phonon branch. To derive an approximate expression for $S_{yy}(q,\omega)$ in this regime,

we consider the variables

$$A=(y(q),\dot{y}(q)) \ . \tag{48}$$

According to Eqs. (40)–(45), we obtain

$$G^{+}_{yy}(q,z)=\beta\omega_T^2\langle y(q)y(-q)\rangle \times\left[z^2+iz\frac{Da}{k_BT}F_{\dot{y}\dot{y}}(q,z)-\omega_T^2\right] \ , \tag{49}$$

where

$$\omega_T^2=\frac{k_BT}{\langle y(q)y(-q)\rangle Da}=\frac{S^{(2)}_{yy}(q)}{S_{yy}(q)} \ , \tag{50}$$

$$F_{\dot{y}\dot{y}}(q,z)=\left\langle \ddot{y}(q)\ Q\frac{i}{z-QLQ}Q\ddot{y}(q)\right\rangle \ , \tag{51}$$

$$P=|y\rangle\frac{1}{\langle yy\rangle}\langle y|+|\dot{y}\rangle\frac{1}{\langle\dot{y}|\dot{y}\rangle}\langle\dot{y}| \ . \tag{52}$$

Neglecting the memory function $F_{\dot{y}\dot{y}}$ in Eq. (49), we have poles at $z=\pm\omega_T$. Because ω_T is related to $S_{yy}(q)$, being proportional to the isothermal susceptibility, we do not yet have the correct high-frequency behavior. For this purpose, we rewrite Eq. (51) in the form

$$F_{\dot{y}\dot{y}}=\left\langle \ddot{y}_1\frac{i}{z-L_1}\ddot{y}_1\right\rangle \ , \tag{53}$$

where

$$\ddot{y}_1=Q\ddot{y}, \quad L_1=QLQ \ , \tag{54}$$

and introduce the projector

$$P_1=|\ddot{y}_1\rangle\frac{1}{\langle\ddot{y}_1|\ddot{y}_1\rangle}\langle\ddot{y}_1| \ , \tag{55}$$

so that

$$F_{\dot{y}\dot{y}}=i\langle\ddot{y}_1|\ddot{y}_1\rangle/z+i\frac{F_{11}}{\langle\ddot{y}_1|\ddot{y}_1\rangle} \ , \tag{56}$$

where

$$\langle\ddot{y}_1|\ddot{y}_1\rangle=\omega_A^2(q)-\omega_T^2(q) \ , \tag{57}$$

$$\omega_A^2(q)=\frac{\langle\ddot{y}(q)\ddot{y}(-q)\rangle}{\langle\dot{y}(q)\dot{y}(-q)\rangle}=\frac{S^{(4)}_{yy}(q)}{S^{(2)}_{yy}(q)} \ . \tag{58}$$

Substitution of Eq. (56) into Eq. (49) yields

$$G^{+}_{yy}(q,z)=\beta\omega_T^2\langle y(q)y(-q)\rangle \times\left[z^2-\omega_T^2-z\frac{\omega_A^2-\omega_T^2}{z+iF_{11}/\langle\ddot{y}_1|\ddot{y}_1\rangle}\right]^{-1} \ . \tag{59}$$

For sufficiently large z, $F_{11}/\langle\ddot{y}_1|\ddot{y}_1\rangle$ is expected to become small. In this high-frequency approximation, we have poles at $z=\pm\omega_A(q)$. More useful expressions might be derived by setting

$$\frac{F_{11}}{\langle\ddot{y}_1|\ddot{y}_1\rangle}=\Sigma'+i\Sigma'' \ , \tag{60}$$

and by neglecting the imaginary part Σ'', giving rise to a shift. In fact, from Eqs. (46), (47), (59), and (60), we then obtain

$$\hat{S}_{yy}(q,\omega)=\frac{S_{yy}(q,\omega)}{S_{yy}(q,t=0)} =\frac{\Sigma'(q)[\omega_A^2(q)-\omega_T^2(q)]\omega_T^2(q)}{[\omega^2-\omega_A^2(q)]^2\omega^2+\Sigma'^2(q)[\omega^2-\omega_T^2(q)]^2} \ . \tag{61}$$

In the high-frequency regime,

$$\omega>>\Sigma' \ ,$$

this expression reduces to

$$\hat{S}_{yy}(q,\omega)=\frac{\Gamma_h(q)\omega_T^2}{(\omega^2-\omega_A^2)^2+\omega^2\Gamma_h^2(q)} \ , \tag{62}$$

where

$$\Gamma_h=\Sigma'(q)\frac{\omega_A^2-\omega_T^2}{\omega_A^2} \ . \tag{63}$$

Provided, that for small values of ω and q, there is no additional pole, from Eq. (61) we may also derive a low-frequency approximation. For

$$\omega<<\Sigma' \tag{64}$$

Eq. (61) reduces to

$$\hat{S}_{yy}(q,\omega)=\frac{\Gamma_l(q)\omega_T^2(q)}{(\omega^2-\omega_T^2)^2+\Gamma_l^2(q)\omega^2} \ , \tag{65}$$

where

$$\Gamma_l(q)=\frac{\omega_A^2-\omega_T^2}{\Sigma'(q)} \ . \tag{66}$$

Clearly, Eq. (65) is expected to be valid only at high temperatures, where a kink contribution is not expected. In this regime, Eq. (62) predicts a resonance close to $\omega=\pm\omega_A$ for large ω values, and a peak close to $\omega=\pm\omega_T$ in the low-frequency regime. From Tables III and V, it is seen that the excitation branch $\omega=\pm\omega_A(q)$ is the expected optic-phonon branch, because $\omega_A(q)$ also results from a Hartree linearization of the equation of motion. In fact, considering the variation of the nonlinear term in Eq. (24),

$$\delta\sin y_l=\cos y_l\delta y_l \ , \tag{67}$$

and replacing $\cos y_l$ by its ensemble average, we obtain in the sG case the linearized equation of motion

$$-\ddot{y}(q)=\omega_0^2\langle\cos y_l\rangle y(q)+\frac{2c_0^2}{a^2}(1-\cos qa)y(q) \ , \tag{68}$$

so that

$$\omega_A^2(q)=\omega_0^2\langle\cos y_l\rangle+\frac{2c_0^2}{a^2}(1-\cos qa)\ . \tag{69}$$

$\omega_A^2(q)$ corresponds to the ratio between the fourth and second frequency moments of $S_{yy}(q,\omega)$ (Table III), satisfying

$$\frac{S_{yy}^{(4)}(q)}{S_{yy}^{(2)}(q)}=\omega_A^2(q)\geq 0\ . \tag{70}$$

Thus the associated phonon branch is an optic one, with a gap given by $\omega_A(q=0)$. Similarly, we might derive the corresponding expressions for the ϕ^4 chain, with ω_4 listed in Table V.

B. Hydrodynamic modes: Heat diffusion and second sound

Considering the continuum limit, the Lagrangian associated with Hamiltonian (1) reads

$$\mathcal{L}=\int dy\, L\ , \tag{71}$$

where

$$L=Da\left[\frac{1}{2}\dot{\phi}^2-\omega_0^2V(\phi)-\frac{c_0^2}{2}\phi_y^2\right]\ . \tag{72}$$

In this limit, where umklapp processes are neglected, not only energy, but also the field momentum are conserved. The conservation laws read

$$\dot{H}=\frac{\partial}{\partial y}J_H,\quad J_H=c_0^2\,\dot{\phi}\phi_y Da\ , \tag{73}$$

$$\dot{\Pi}=-\frac{\partial}{\partial y}J_\Pi,\quad J_\Pi=L+Dac_0^2\phi_y^2\ , \tag{74}$$

where

$$H=Da\left[\frac{\dot{\phi}^2}{2}+\omega_0^2V(\phi)+\frac{c_0^2}{2}\phi_y^2\right]\ , \tag{75}$$

$$\Pi=-Da\,\dot{\phi}\phi_y\ . \tag{76}$$

These conservation laws are easily verified by inspection, and are a consequence of Noether's theorem. Energy conservation also holds in the discrete case, while the conservation of field momentum is approximate only, because umklapp processes are not taken into account. Nevertheless, the neglect of these processes is justified at sufficiently low temperatures.

To estimate the second-sound frequency, we consider the energy density H and the field momentum as dynamic variables.[15] Neglecting in a first step the memory functions, we obtain from Eq. (40),

$$G_{HH}^{+}(q,z)=-\beta\langle H(q)H(-q)\rangle\frac{\omega_{ss}^2}{Z^2-\omega_{ss}^2}\ , \tag{77}$$

where

$$\omega_{ss}^2(q)=\frac{|\langle\Pi(q)\dot{H}(-q)\rangle|^2}{\langle H(q)H(-q)\rangle\langle\Pi(q)\Pi(-q)\rangle}\ , \tag{78}$$

ω_{ss} being an estimate for the second-sound frequency. Equation (78) might be further simplified, with the aid of Eqs. (73)–(76), yielding, in the limit $q\to 0$,[14]

$$\omega_{ss}^2(q)=a^2q^2\frac{(Dc_0^2/a)^2\sum_{q'}a^2q'^2\langle|y(q')|^2\rangle}{Dac_VT}$$

$$=\frac{\langle\dot{\mathcal{H}}(q)\dot{\mathcal{H}}(-q)\rangle}{\langle\mathcal{H}(q)\mathcal{H}(-q)\rangle}\ . \tag{79}$$

Here we replaced $\langle\mathcal{H}(q)\mathcal{H}(-q)\rangle$ by

$$\langle\mathcal{H}(q)\mathcal{H}(-q)\rangle=c_Vk_BT^2 \tag{80}$$

for $q\to 0$, where c_V is the specific heat at constant length. Owing to the neglect of the memory function, we assumed second sound to be an extremely well-defined excitation. Second sound, however, is a more delicate phenomenon, expected to occur only in a temperature window. At the upper limit, it becomes overdamped due to umklapp processes, and goes over to heat diffusion. At the lower limit, there are no more sufficiently dissipative processes to maintain local thermal equilibrium.[15] Consequently, a full discussion of second sound would require an evaluation of the memory function matrix. Here we adopt the predictions of phonon hydrodynamics, where the second-sound resonance is given by[14]

$$\hat{S}_{HH}(q,\omega)=\frac{S_{HH}(q,\omega)}{S_{HH}(q,t=0)}$$

$$=\frac{2\omega_{ss}^2(q)\Gamma(q)}{\omega^2-\omega_{ss}^2(q)^2+\omega^2\Gamma^2(q)}\ . \tag{81}$$

The half-width $\Gamma(q)$ is related to the phonon relaxation time for normal (τ_N) and umklapp processes (τ_u) by[14]

$$\Gamma(q)=\tau_u^{-1}+\omega_{ss}^2(q)\tau_N\ . \tag{82}$$

Equation (81) is certainly an approximation, because only the damping part, and not the shift associated with the memory function, is taken into account.

C. Low-temperature approximation for kink-insensitive dynamic form factors

Our discussion of the static properties revealed that, in the low-temperature regime, kink-insensitive static form factors can be well described by anharmonic perturbation theory. Here we extend this approach to the corresponding dynamic form factors. First, we treat the sG chain.

1. sG chains

Using the Hartree "harmonic" approximation, we have

$$y_l(t)=\frac{1}{\sqrt{2N}}\sum_q \exp iqal \times [B_q \exp i\omega_q t + B_q^* \exp(-i\omega_q t)] \ , \tag{83}$$

where

$$\langle B_q B_q \rangle = \langle B_q^* B_q^* \rangle = 0 \ , \tag{84}$$

$$\langle B_q B_{q'}^* \rangle = \frac{k_B T}{Da\,\omega_q^2}\delta_{qq'} \ , \tag{85}$$

$$\omega_q^2 = \omega_0^2 \langle \cos y \rangle + 2\frac{c_0^2}{a^2}(1-\cos qa) \ . \tag{86}$$

Assuming the magnitude of the displacements to be small, we replace $\cos y_l$ by

$$\cos y_l \approx 1 - y_l^2/2 \ , \tag{87}$$

so that

$$S_{cc}(q,\omega) \approx \tfrac{1}{4}\pi\left(\frac{k_B T}{Da}\right)^2 \frac{1}{N} \times \sum_{q'} \frac{1}{\omega_q^2 \omega_{q-q'}^2} [\delta(\omega \pm (\omega_{q'} + \omega_{q-q'})) + \delta(\omega \pm (\omega_{q'} - \omega_{q-q'}))] \ . \tag{88}$$

The associated static form factor $S_{cc}(q,t=0)$ is correct in the limit $T \to 0$ to leading order.[1] For finite q values, Eq. (88) predicts a low-frequency resonance due to the difference process, and a high-frequency resonance associated with the sum process.

This approximation can also be applied to $S_{HH}(q,\omega)$, by replacing the single-site potential by $\omega_0^2 y_l^2/2$. The result is

$$S_{HH}(q,\omega) = \frac{\pi}{8}\left(\frac{k_B T}{Da}\right)^2 \frac{1}{N}\left\{\sum_{q'}\left[\frac{1}{2}\left[3+4\frac{\omega_{q-q'}}{\omega_{q'}}+\frac{\omega_{q-q'}^2}{\omega_{q'}^2}\right]\delta(\omega \pm (\omega_{q'} - \omega_{q-q'}))\right] + \left[\frac{1}{2}\left[3-4\frac{\omega_{q-q'}}{\omega_{q'}}+\frac{\omega_{q-q'}^2}{\omega_{q'}^2}\right]\delta(\omega \pm (\omega_{q'} + \omega_{q-q'}))\right]\right\} \ . \tag{89}$$

The resulting static form factor $S_{HH}(q,t=0)$ is again correct to leading order in the limit $T \to 0$.[1] It should be kept in mind, however, that in these approximate expressions [Eqs. (88) and (89)] lifetime effects have been neglected, so that the establishment of local equilibrium, in terms of phonon normal processes, is not guaranteed. It is important to emphasize this point, to avoid a possible confusion in the interpretation of the low-frequency resonance due to the first term in Eq. (89) and second sound [Eq. (81)].

2. ϕ^4 chain

To derive the corresponding results for the ϕ^4 chain, we start from the equation of motion, resulting from Hamiltonian (1) and single-site potential (3),

$$-\ddot{y}_l = -\Delta y_l + B y_l^3 + \frac{c_0^2}{a^2}(2y_l - y_{l+1} - y_{l-1}) \ . \tag{90}$$

Following Ref. 1, we introduce

$$y_l = y_0 + \delta y_l \ , \tag{91}$$

where y_0 denotes the mean displacement in one of the wells. Substitution of Eq. (91) into Eq. (90) then yields, by taking the average,

$$y_0^2 = \frac{\Delta}{B} - 3\langle \delta y_l^2 \rangle \ , \tag{92}$$

and by invoking the Hartree linearization of $(\delta y_l)^3$,

$$\omega_q^2 = 2\Delta - 6B\langle (\delta y_l)^2 \rangle + \frac{c_0^2}{a^2}2(1-\cos qa) \ . \tag{93}$$

Using Eqs. (83)–(85) and (92), we then obtain

$$S_{y^2 y^2}(q,\omega) = 4\pi\left(\frac{k_B T}{Da}\right)^2 \frac{1}{N}\sum_{q'} \frac{1}{\omega_q^2 \omega_{q-q'}^2} [\delta(\omega \pm (\omega_{q'} + \omega_{q-q'})) + \delta(\omega \pm (\omega_{q'} - \omega_{q-q'}))] + 4y_0^2 \frac{k_B T}{Da\,\omega q^2}\pi[\delta(\omega+\omega_q) + \delta(\omega-\omega_{q'})] \ , \tag{94}$$

where

$$y_0^2 = \frac{\Delta}{B} - 3\langle(\delta y_l)^2\rangle = \frac{\Delta}{B} - \frac{3}{2}\frac{k_B T}{Da}\left[1+2\left(\frac{d}{a}\right)^2\right]^{1/2} , \quad (95)$$

and ω_q is given by Eq. (93). In contrast to the sG case [Eq. (88)], $S_{y^2_{y^2}}(q,\omega)$ does not exhibit two-phonon contributions only. Due to the nonvanishing mean displacment in one of the wells, there is also a one-phonon contribution. As in the sG case, the static form factor $S_{y^2_{y^2}}(q,t=0)$, resulting from Eq. (94), is correct up to second order in T in the limit $T\to 0$.[1] For finite q values, Eq. (94) predicts a low-frequency resonance due to the difference process and two high-frequency peaks, associated with the one-phonon branch resonance and the two-phonon processes. We also note that for small q values, $S_{HH}(q,\omega)$ is given by Eq. (89) also in the present case, but with ω_q replaced by Eq. (93). As in the sG case, the low-frequency resonances appearing in $S_{y^2_{y^2}}(q,\omega)$ [Eq. (94)] and $S_{HH}(q,\omega)$ due to the two-phonon difference process, should not be confused with second sound.

D. High-temperature approximations

As noted above, in the limit $T\to\infty$, the sG chain behaves in a particularly simple manner, because the periodic single-site potential becomes gradually irrelevant. That is to say, the harmonic approximation becomes exact in this limit, with the important feature, however, that the amplitude of the oscillations becomes very large. The ϕ^4 chain, on the other hand, tends to a set of independent quartic oscillators.

1. sG chain

As a consequence, for $\beta E_k^0 \ll 1$, the sG chain behaves as a weakly interacting phonon gas, associated with nearly harmonic large-amplitude oscillations. Here, kinks no longer play a role, so that the dynamic form factor $S_{yy}(q,\omega)$ should be well approximated by the high- [Eq. (62)] or low-frequency [Eq. (65)] approximation. From the ratio

$$\frac{\hat{S}_{yy}(q,\omega_T)}{\hat{S}_{yy}(q,\omega_A)} = \frac{\Sigma'(q)(\omega_A^2-\omega_T^2)}{\omega_T^2} = \frac{\Sigma'(q)\omega_0^2\langle\cos y\rangle}{2(c_0^2/a^2)(1-\cos qa)} \quad (96)$$

as obtained from Eqs. (61), (50), Table III, and the high-temperature expression for $S_{yy}(q,t=0)$,

$$S_{yy}(q,t=0) = \frac{k_B T a}{2Dc_0^2(1-\cos qa)} , \quad (97)$$

it is seen that the low-frequency regime will apply for small, and the high-frequency approximation at large wave numbers. In fact, the ratio (96) becomes large for small wave numbers.

Since the amplitude of the nearly harmonic oscillations becomes very large, for $\beta E_k^0 \ll 1$, the evaluation of other dynamic form factors, such as $S_{cc}(q,\omega)$, is quite nontrivial. Nevertheless, $y_l(t)$ evolves almost according to the harmonic approximation [Eq. (83)], so that $S_{cc}(q,\omega)$ can be evaluated numerically on this basis.

2. ϕ^4 chain

The high-temperature behavior of the ϕ^4 chain is more complicated, because the system tends to a set of quartic independent oscillators, with Hamiltonian

$$H = \sum_l Da\left(\frac{\dot{y}_l^2}{2} + \frac{B}{4}y_l^4\right) . \quad (98)$$

Nevertheless, $S_{yy}(q,\omega)$ can be calculated exactly in this limit. The result is[16]

$$S_{yy}(\omega) = \frac{1}{Z}\frac{32\pi^2}{B}\sum_{\substack{m\geq 1\\ \text{odd}}}^{\infty}\frac{1}{m\cosh^2 m\pi/2}\frac{\omega^4}{\eta_m^4} \times \exp\left(-\frac{\omega^4}{\eta_m^4 k_B T}\right) , \quad (99)$$

where

$$\eta_m = \frac{\pi}{\sqrt{2}K(1/\sqrt{2})}\left(\frac{B}{(Da)^2}\right)^{1/4} , \quad (100)$$

$$Z = \frac{2\sqrt{2}K(1/\sqrt{2})\Gamma(3/4)}{(Da)^{1/2}B^{1/4}}(k_B T)^{3/4} , \quad (101)$$

$K(k)$ being the complete elliptic function of the first kind. For $T\to\infty$, where Eq. (99) applies to the ϕ^4 chain, the resonance due to the energy-dependent oscillation frequency, becomes very broad.

E. Ideal kink-gas approximation

The idea of using an ideal gas of kinks to construct approximate expressions for dynamic form factors has been employed by various authors.[3–6] From the behavior of the static properties, we know, however, that this approach at best, is valid only at low temperatures and for kink-sensitive properties.

In this subsection, we formulate an ideal kink-gas phenomenology to deriye the kink contribution to

kink-sensitive dynamic form factors. For this purpose, we have to evaluate the kink contribution to the correlation functions

$$S_{AA}(y,t)=\langle \delta A[\phi(y,t)]\delta A[\phi(0,0)]\rangle \ , \quad (102)$$

where

$$\Delta A = A[\phi]-\langle A[\phi]\rangle \ . \quad (103)$$

The variables A of interest are functions of the field ϕ. Assuming N indistinguishable kinks of energy [Eq. (8)],

$$E_j = E_j^0\gamma_j+\Sigma_j=(E_j^{02}+P_j^2c_0^2)^{1/2}+\Sigma_j \ , \quad (104)$$

and momentum

$$P_j = M_j^0 v_j, \quad E_j^0 = M_j^0 c_0^2 \ , \quad (105)$$

the kink contribution to the Eq. (102) can be estimated by

$$S_{AA}^{(k)}(y,t)=\frac{1}{Z_k}\sum_{N=0}^{\infty}\frac{1}{N!}\prod_{j-1}^{N}\frac{\alpha}{\nu L}\int dy_j\int dP_j\exp(-\beta E_j)\delta A[\phi_k(y,t)]\delta A[\phi_k(0,0)] \ , \quad (106)$$

where

$$\alpha=(2\pi)^{1/2}(\beta Da)^{1/2}Na, \quad L=Na \ , \quad (107)$$

$$\Sigma_j=-\tfrac{1}{2}k_BT\ln\beta Da\,\omega_0^2-k_BT\sigma \ ,$$
$$Z_k=\sum_{N=0}^{\infty}\frac{1}{N!}\prod_{j=1}^{N}\frac{\alpha}{\nu}\int dP_j\exp(-\beta E_j) \ , \quad (108)$$

ν being a temperature-independent phase-reduction factor, and Σ_j [Eq. (104)] the change of the phonon free energy in the presence of a kink. For a complete discussion of the ideal kink-gas approximation and its application to static properties, we refer to Currie *et al.*[17]

To perform the summation and integrations in Eq. (106), we have to specify the dynamic variable $A[\phi]$ and its decomposition into kink solutions. This decomposition should be guided by the following requirements: (a) In integrable systems, it should be consistent with the solution of the initial-value problem. (b) The static form factors $S_{AA}(y,t=0)$ should reproduce the exact transfer integral results to leading order in the limit $\beta E_k^0 >> 1$, where the ideal kink-gas picture is expected to apply. Because the second condition can be verified only by quantitative comparison, we next consider the sG and ϕ^4 systems separately, and concentrate on kink-sensitive variables A.

1. sG system

We suppose, as is justified for fully integrable systems, that for arbitrary initial conditions, the time evolution of the field $\phi(y,t)$ can be decomposed into a superpositon of solitons, as $t\to\infty$. The kink contribution can then be expressed as

$$\phi_k(y,t)-\sum_j\Phi_{kj}(\gamma_j(y-y_j-v_jt)) \ . \quad (109)$$

The further ansatz is usually adopted,

$$A[\Phi_k(y,t)]\simeq\sum_j A[\phi_{kj}(\gamma_j(y-y_j-v_jt))] \ . \quad (110)$$

It is important to emphasize that Eqs. (109) and (110) are equivalent only if A is a linear function of ϕ, i.e., $A=\phi$, ϕ_x, ϕ_t, etc. Before substituting Eq. (110) into Eq. (106), we make the further approximation

$$A[\phi_k(y,t)]A[\phi_k(0,0)]$$
$$=\sum_j A[\Phi(\gamma_j(y-y_j-v_jt))][A\phi(-y_j\gamma_j)] \ , \quad (111)$$

which is in the spirit of the ideal kink-gas picture, where kink correlations are neglected.

Substitution of Eq. (111) into (106) then yields for

$$\beta E_k^0 >> 1 \ , \quad (112)$$

$$S_{AA}^k(q,t)=n_k(T)\frac{\int dv\,\gamma^3\exp(-\beta\gamma E_k^0)|A(q\gamma^{-1})|^2\gamma^{-2}e^{iqvt}}{\int dv\,\gamma^3\exp(-\beta\gamma E_k^0)} \ , \quad (113)$$

where

$$A(Q)=\int_{-\infty}^{+\infty}\exp(-iQy)A[\phi_k(y)]dy \ , \quad (114)$$

$$n_k(T)=\frac{\alpha}{\nu L}\left[\frac{2E_k^0}{c^0}\right]\left[\frac{2\pi}{\beta E_k}\right]^{1/2}\exp[-\beta(E_k^0+\Sigma_k)]$$
$$=(2\pi)^{-1/2}\left[\frac{4}{d}\right](\beta E_k^0)^{1/2}\exp(-\beta E_k^0) \ . \quad (115)$$

In deriving the total kink density n_k, we used Eq. (108) with $\nu=1$ and $\sigma=\ln 2$.[17] The kink form factor associated with the variable A is denoted by $A(Q)$. Introducing the velocity distribution of an ideal relativistic kink gas, defined by

$$P(v)=\frac{1}{P_0}\gamma^3\exp(-\beta E_k^0\gamma) \ , \quad (116)$$

where P_0 is given by

$$\int_{-c_0}^{+c_0} P(v)\,dv = 1 \ , \tag{117}$$

Eq. (113) may be rewritten in the form

$$S_{AA}^k(q,t) = n_k(T)\frac{1}{P_0}\int P(v)\gamma^{-2}|A(q\gamma^{-1})|^2 e^{iqvt}\,dv \ , \tag{118}$$

so that the static form factors and dynamic form factors are given by

$$S_{AA}^k(q,0) = S_{AA}(q) = n_k(T)\frac{1}{P_0}\int P(v)\gamma^{-2}|A(q\gamma^{-1})|^2\,dv \ , \tag{119}$$

$$\hat{S}_{AA}^k(q,\omega) = \frac{S_{AA}(q,\omega)}{S_{AA}(q,t=0)} = \frac{2\pi}{N_0 q c_0} P\left(\frac{\omega}{q}\right)\left[\gamma\left(\frac{\omega}{q}\right)\right]^{-2}\left|A\left(q\gamma^{-1}\left(\frac{\omega}{q}\right)\right)\right|^2 \ , \tag{120}$$

where

$$N_0 = \int_{-1}^{+1} P(x)|A(q\gamma^{-1}(x))|^2\gamma^{-2}(x)\,dx \ . \tag{121}$$

In the limit $\beta E_k^0 >> 1$ and $T \to 0$, the relativistic velocity distribution (116) reduces to

$$P(v) = \left(\frac{\beta E_k^0}{2\pi}\right)^{1/2}\frac{1}{c_0}\exp\left(-\frac{\beta E_k^0}{2c_0^2}v^2\right) \ , \tag{122}$$

and Eq. (120) simplifies to

$$\hat{S}_{AA}^k(q,\omega) = \left(\frac{\beta E_k^0}{2\pi}\right)^{1/2}\frac{1}{c_0}\exp\left(-\frac{\beta E_k^0\omega^2}{2c_0^2 q^2}\right) \ . \tag{123}$$

This expression is independent of the form factor $A(Q)$ and predicts a central peak (a resonance centered about $\omega = 0$ for fixed q) due to the kinks. At higher temperatures, however, where Eq. (120) applies, this central peak may split, as the temperature dependence of the velocity distribution, shown in Fig. 1, reveals.

Before discussing the dynamic form factors in more detail, it is necessary to check the validity of the resulting static form factors by comparison with the corresponding transfer-integral results, in the limits $\beta E_k^0 >> 1$, and $T \to 0$, where Eq. (119) reduces to

$$S_{AA}^k(q) = n_k(T)|A(q)|^2 \ . \tag{124}$$

Some of the relevant kink form factors are listed in Table VII. Substitution of these form factors into Eq. (124) in the limit $q \to 0$, yields the results summarized in Table VIII. For comparison, we included

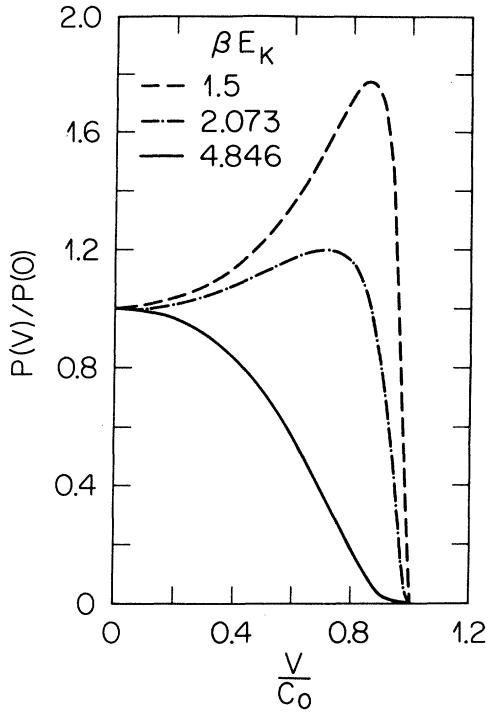

FIG. 1. Temperature dependence of the relativistic velocity distribution [Eq. (116)].

the corresponding leading term of the transfer-integral expression.[1] It is seen that the ideal kink-gas approach reproduces the correct results for $S_{\phi\phi}(q)$ and $S_{\phi_y\phi_y}(q)$ but fails for $S_{cc}(q)$ and $S_{ss}(q)$, which are not sensitive to kinks in leading order and where $A[\phi]$ is nonlinear and periodic ($A[\phi] = \cos\phi$, $\sin\phi$). These comparisons then indicate that the ideal kink-gas picture, in the sG system leads to the correct kink-dominated properties, such as $S_{yy}(q)$. For $S_{cc}(q)$ and $S_{ss}(q)$, where A is a periodic and nonlinear function of ϕ, this is not the case, because phonon and anharmonic contributions dominate the low-temperature behavior.

TABLE VII. Kink form factors [Eq. (114)] for the sG system, with $\phi_k = 4\tan^{-1}\exp(\pm y/d)$, $d = c_0/\omega_0$.

$A[\phi_k]$	$A(Q)$
ϕ_k	$\frac{2\pi}{Q}\,\mathrm{sech}(\pi/2)Qd$
ϕ_{kx}	$2\pi\gamma\,\mathrm{sech}(Q\pi d/2)$
$\cos\phi_k$	$-4d\frac{(\pi/2)Qd}{\sinh(\pi/2)Qd}$
$\sin\phi_k$	$4d\frac{(\pi/2)Qd}{\cosh(\pi/2)Qd}$

TABLE VIII. Comparison of static form factors as obtained from the ideal kink-gas approach and the transfer-integral technique in the limits $q \to 0$ and $T \to 0$.

$S^k_{AA}(q)$	$S_{AA}(q)$
$S^k_{\phi\phi}(q) = S_{yy}(q) = n_k(T) c_0 4\pi^2 q^{-2}$	$S_{yy}(q) = n_k(T) c_0 4\pi^2 q^{-2}$
$S^k_{\phi_y \phi_y}(q) = q^2 S^k_{\phi\phi}(q)$	$q^2 S_{yy}(q)$
$S^k_{cc}(q) = n_k(T) 16 c_0 d^2$	$S_{cc}(q) = 8\left[\frac{k_B T}{E_k^0}\right]^2 \frac{d}{a}$
$S^k_{ss}(q) = n_k(T) 4 d^4 \pi^2 c_0 q^2$	$S_{ss}(q) = \frac{k_B T}{Da\omega_0^2}$

In view of this, one expects that among the dynamic form factors considered here, only $S_{yy}(q,\omega)$ is reasonably approximated by the ideal kink-gas picture. Nevertheless, even though the exact static form factor is reproduced, lifetime effects are not yet incorporated. In Fig. 2, we show the ω dependence of $S^k_{yy}(q,\omega)$ for some fixed q values and some characteristic temperatures. The parameters correspond to those in Ref. 1:

$$M=1, \quad a=1, \quad D=Ma=1 \ , \tag{125}$$

$$d^2 = \frac{c_0^2}{\omega_0^2} = 29.22, \quad \omega_0^2 = 1 \ , \tag{126}$$

$$E_k^0 = 8D\omega_0 c_0 = 43.244 \ ,$$

implying the units

$$[k_B T] = [c_0^2] = [\omega_0^2] \ . \tag{127}$$

The results shown in Fig. 2 clearly illustrate the central-peak character and its splitting for small βE_k^0 values due to the relativistic effects. Another important feature is the strong q dependence. To summarize, the ideal kink-gas picture presented here predicts, in the sG system, a kink resonance in $S_{yy}(q,\omega)$ restricted to small ω and q values. For $\beta E_k^0 >> 1$, it is centered about $\omega = 0$, and splits the larger βE_j^0 due to relativistic effects. In the limit $T \to 0$, the half-width behaves according to Eq. (123) as

$$\omega_{1/2} = c_0 q \left[\frac{2k_B T \ln z}{E_k^0}\right]^{1/2} \ , \tag{128}$$

predicting a narrowing of the kink central peak with decreasing temperature.

The ϕ^4 system is not exactly integrable, and for topological reasons, a kink can be followed only by an antikink. It is not surprising, therefore, that for $A = \phi$, ϕ_x, and ϕ^2 the ansatz (109) leads to incorrect static form factors. To account for the topological constraint stated above, it is essential to use the product ansatz[5]

$$\phi(y,t) = \frac{1}{\sqrt{b}} \prod_{i=1}^{N} \tanh[\gamma_i \delta(y + y_i - v_i t)] \ , \tag{129}$$

where

$$\delta = \frac{1}{d}\sqrt{b/2} \ . \tag{130}$$

The corresponding single kink solution is given in Table I. Substitution of Eq. (129) into Eq. (106)

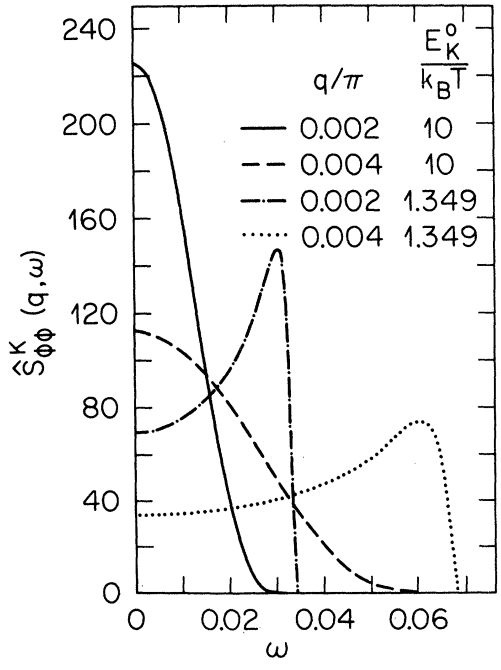

FIG. 2. $\hat{S}^k_{\phi\phi}(q,\omega)$ [Eq. (120)] for some fixed q values and temperatures for the sG system with parameters given by Eq. (126).

yields in the limit

$$\beta E_k^0 >> 1 \ , \tag{131}$$

$$S^k_{\phi\phi}(y,t) = s^k_{yy}(y,t)$$
$$= \frac{1}{b}\exp\left[-\frac{\alpha}{\nu L}\int_{-c_0}^{+c_0} d v\, M_k^0 \gamma^3 \{\exp[-\beta(E_k^0\gamma+\Sigma_k)]\}2(y-vt)\coth(y-vt)\right] \ , \tag{132}$$

for that for $T\to 0$,

$$S^k_{yy}(y,0) = \frac{1}{b}\exp\left[-\frac{|y|}{\xi_{yy}}\right], \quad \xi_{yy} = \frac{1}{2n_k} \ . \tag{133}$$

This result for the static correlation function agrees with the transfer-integral result, because

$$\xi_{yy} = \frac{1}{2n_k} = \frac{k_B T}{2t_0\omega_0^2} \ , \tag{134}$$

where t_0 is the tunnel splitting, and ξ_{yy} denotes the correlation length in the limit $T\to 0$. According to Eqs. (108) and (115), the kink density is given by

$$n_k = (2\pi)^{-1/2} 4(\tfrac{3}{2})^{1/2}\frac{1}{d}(\beta E_k^0)^{1/2}\exp(-\beta E_k^0) \ , \tag{135}$$

where we used[17]

$$\sigma = \ln[4(\tfrac{3}{2})^{1/2}], \quad \nu = 2 \ . \tag{136}$$

Having justified the ansatz (129), we return to the time-dependent correlation function [Eq. (132)], which is fundamentally different from the sG case [Eq. (112)]. Because it is cumbersome to evaluate the integral and to perform the Fourier transform, in Fig. 3 we present numerical results for the resulting dynamic form factor $S^k_{yy}(q,\omega)$, for

$$\omega_0^2 = 0.05, \quad c_0^2 = 0.5, \quad b = \tfrac{20}{3} \ ,$$
$$E_k^0 = \frac{2\sqrt{2}}{3} Da\,\omega_0 c_0 \frac{1}{b} = 0.0224 \ , \tag{137}$$

and α, Σ, and ν given by Eqs. (107), (108), and (136). For a definition of the units, we refer to Eq. (127). As in the sG system, the ideal kink-gas approximation predicts a kink resonance, restricted to small q and ω values. In contrast to the sG case, $S^k_{yy}(q,\omega)$ is well behaved in the limit $q\to 0$, since the particles are localized in the double-well single-site potential. Some analytical insight might be obtained for $T\to 0$, $|y|\to\infty$, $t\to\infty$, and $\delta(y-vt) >> 1$, where Eq. (32) reduces to

$$S^k_{yy}(y,t) = \frac{1}{b}[\exp(-2n_k|y|)]\left[\exp\left(-\frac{|t|}{\tau}\right)\right] \ , \tag{138}$$

where

$$\frac{1}{\tau} = \frac{n_k\sqrt{2}c_0}{\sqrt{\pi}(E_k^0)^{1/2}} = \frac{4(\frac{3}{2})^{1/2}\omega_0}{\pi}\exp(-\beta E_k^0) \ . \tag{139}$$

On Fourier transforming [Eq. (138)] we obtain the approximate result

$$\hat{S}^k_{yy}(q,\omega) = \frac{1/\tau}{\omega^2 + 1/\tau^2} \ , \tag{140}$$

with

$$S^k_{yy}(q) = \frac{1}{b}\frac{2n_k}{q^2+(2n_k)^2} \ , \tag{141}$$

in agreement with Eq. (133). Equation (140) predicts a kink central peak with heights, growing exponentially as we lower the temperature [Eq. (139)], and a half-width

$$\omega_{1/2} = 1/\tau \tag{142}$$

becoming narrower with decreasing temperature. Comparison with the numerical results shown in Fig.

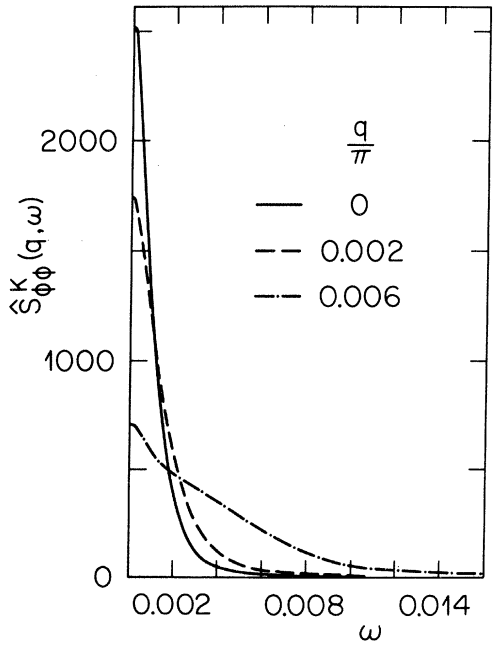

FIG. 3. $\hat{S}^k_{\phi\phi}(q,\omega)$ resulting from Eq. (132) for some fixed q values and $k_B T = 0.00344$ ($\beta E_k^0 = 6.5$) for the ϕ^4 system.

3 reveals that this approximation is quite good for $q=0$ but fails to account for the strong q dependence. As in the sG case, it should be kept in mind that, in the ideal kink-gas approximation, lifetime effects are neglected.

V. MOLECULAR-DYNAMICS TECHNIQUE

In the conventional molecular-dynamics technique,[18,19] one solves the set of coupled Newton's equations associated with a given Hamiltonian according to a set of difference equations with a time increment. This set of difference equations approximates Newton's equations. Starting from given initial conditions for the positions and velocities, the particles are then allowed to move, and the time evolution of their canonical variables $(X_l,\dot{X}_l)$ are calculated. Assuming the system is ergodic, estimates for microcanonical ensemble averages may be obtained in terms of time averages.

It would be preferable to have a molcular-dynamics technique, simulating a canonical ensemble, as most experiments are performed at constant global temperature. This was achieved by considering, in place of the Newton's equations, the coupled set of Langevin equations[20]

$$M\ddot{X}_l=-\frac{\partial\mathcal{H}}{\partial X_l}-\Gamma M\dot{X}_l+\eta_l(t) \ , \tag{143}$$

where

$$\langle\eta_l(t)\eta_{l'}(t')\rangle=2M\Gamma k_BT\delta(t-t')\delta_{ll'} \ . \tag{144}$$

Here, it is assumed that the particles suffer collisions with much lighter ones which represent the heat bath defining the temperature T. The collisions are described by the friction $\Gamma M\dot{X}_l$ and a random force $\eta_l(t)$. It may be shown that the stationary solution of the associated Fokker-Planck equation is the canonical distribution function

$$P_{eq}(\dot{X}_1,\ldots,\dot{X}_N,X_1,\ldots,X_N)=\exp\left[-\frac{1}{k_BT}\mathcal{H}\right] \ . \tag{145}$$

Starting from initial values for positions and velocities, the particles are then allowed to move under the influence of the computer-generated random force. The temporal evolution of the variables are then calculated with a set of difference equations approximating the Langevin equations (143). On this basis, one obtains

$$X_l(t),\ \dot{X}_l(t),\ \ddot{X}_l(t),\ \ldots \ . \tag{146}$$

For a detailed description of the algorithm and the random-force generation, we refer to Ref. 20. The system is then allowed to age, or, in other words, to reach equilibrium. After this interval, the subsequent 10^5 steps are used to perform time averages representing canonical ensemble averages.

From the Langevin equations (143), it is obvious that the dynamic properties will be modified, in particular, owing to the damping term. To reduce this modification, Γ must be chosen in such a way that

$$\frac{1}{\Gamma}>>\tau_c \ , \tag{147}$$

where τ_c denotes the characteristic time of the dynamics. This guarantees that the excitations do not become overdamped owing to the friction term. Another important constraint on Γ evolves from the energy conservation of a Hamiltonian system. Since our system evolves according to the Langevin equation, it follows that

$$\frac{d\mathcal{H}}{dt}=\sum_l\frac{\partial\mathcal{H}}{\partial M\dot{X}}M\ddot{X}_l+\frac{\partial\mathcal{H}}{\partial X_l}\dot{X}_l$$
$$=-\sum_l[\Gamma M\dot{X}_l^2-\dot{X}_l\eta_l(t)] \ . \tag{148}$$

Consequently, energy is not conserved because the Hamiltonian system is in contact with the heat bath. To avoid artificial features due to the random-noise pulses, the mean time between two pulses must be small compared to τ_c. In this case, we may average Eq. (148) over some pulses. This leads to

$$\frac{d\mathcal{H}}{dt}=-\Gamma[2E_{\rm kin}(t)-Nk_BT]=-\delta E_k(t) \ . \tag{149}$$

With the ansatz

$$\delta E_k(t)=\alpha\exp(-t/\tau) \tag{150}$$

and

$$\frac{d\mathcal{H}}{dt}=\frac{d\mathcal{H}}{d\delta E_k}\frac{d\delta E_k}{dt}=\frac{d\mathcal{H}}{dT}\frac{dT}{d\delta E_k}\frac{d\delta E_k}{dt}\approx\frac{2c_V}{k_B}\frac{d\delta E_k}{dt} \ , \tag{151}$$

we find

$$\tau=\frac{c_V}{k_B}\frac{1}{\Gamma} \ , \tag{152}$$

where c_V is the specific heat. Accordingly, energy is almost conserved within the characteristic time τ_c, provided that

$$\tau=\frac{c_V}{k_B}\frac{1}{\Gamma}>>\tau_c \ . \tag{153}$$

Moreover, owing to the fact that the system evolves according to the Langevin equation, the time interval $\tau_{\rm ch}$ over which the evolution is followed, must be larger than τ so that

$$\tau<<\tau_{\rm ch} \ . \tag{154}$$

Combining inequalities (153) and (154), we finally obtain

$$\tau_{\rm ch} >> \frac{c_V}{k_B \Gamma} >> \tau_c \ . \tag{155}$$

From this relation, it becomes evident that energy can be almost conserved provided Γ and the chain length $\tau_{\rm ch}$ are chosen appropriately. An exception is very close to T_c, where the characteristic time τ_c becomes very long.

In the calculations presented here, we have considered systems of 1000 particles subjected to periodic boundary conditions. In the time interval, where time averages were performed, Γ was chosen as

$$\Gamma = 0.004 \ . \tag{156}$$

For a discussion of the algorithms we refer to Ref. 20.

VI. MOLECULAR-DYNAMICS RESULTS: sG CHAIN

In this section, we shall present and discuss some results for the dynamic form factors characterizing the excitation spectrum of the sG chain. The data will be given in terms of the reduced dynamic form factors

$$\hat{S}_{AA}(q,\omega) = \frac{S_{AA}(q,\omega)}{S_{AA}(q,t=0)} \ , \tag{157}$$

where $S_{AA}(q,\omega)$ was defined in Eq. (11). For a definition of the variables A and the notation, we refer to Table II. Choice of the model parameters was given in Eqs. (125)–(127). This choice guarantees that, for

$$k_B T << \omega_0^2 Da \left[\frac{d}{a}\right]^2 = 29.22 \ , \tag{158}$$

the system belongs to the strong coupling regime, where the static properties can be estimated in terms of the pseudo-Schrödinger equation, to which the transfer-integral equation reduces. The temperatures to be considered are listed in Table IX and marked by arrows in Fig. 4, where we show the temperature dependence of the specific heat to illustrate the low-, intermediate-, and high-temperature regimes. The approximate treatments discussed in Sec. IV are either valid in the low-temperature regime, $k_B T \lesssim 5$, or at high temperatures, $k_B T \gtrsim 20$. Accordingly, in the intermediate regime, where the specific heat exhibits the maximum (Fig. 4), the predictions of the approximate approaches must be treated with caution. In order to guarantee thermal equilibrium, it was not possible to perform MD for lower temperatures, because the kink density is too small in a system of 10^3 particles.

TABLE IX. Gap frequencies $\omega_A(q=0)$ [Eq. (69)] transfer-integral estimates for $\langle \cos y_l \rangle$ and estimates for the second-sound frequency [Eq. (79)].

$k_B T$	$\frac{E_k^0}{k_B T}$	$\langle \cos y_l \rangle$	$\omega_A(q=0)$	$\omega_{ss}(q_{\rm red}=0.002)$
8.924	4.85	0.566	0.75	0.032
12.5	3.46	0.354	0.60	0.033
20.86	2.07	0.133	0.36	0.034
43.244	1	0.033	0.18	0.034

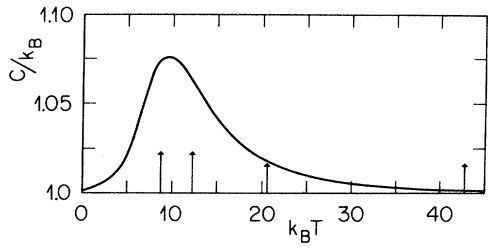

FIG. 4. Temperature dependence of the specific heat for the sG chain with parameters given by Eqs. (125)–(127). The arrows mark the particular temperatures, where MD studies of the dynamic form factors have been performed.

A. $\hat{S}_{yy}(q,\omega)$

According to the kink-gas picture (Fig. 2), at low temperatures and small q and ω values, we expect, a resonance due to the kinks. It will be a peak centered about zero frequency, which is expected to split with increasing temperature, due to relativistic effects.

Numerical results for $\hat{S}_{yy}(q,\omega)$ are shown in Fig. 5 for $k_B T = 8.924$, and in Figs. 5 and 6 for $k_B T = 12.5$. For small wave numbers and frequencies, the spectrum (Figs. 5 and 6) is dominated by a low-frequency resonance, which is seen to split with increasing temperature. There is also a high-frequency peak, becoming stronger with increasing wave number (Fig. 6) and persisting up to the Brillouin zone boundary. Before turning to this feature, let us compare the low-frequency resonance with the predictions of the ideal kink-gas phenomenology. For this purpose, we calculated the kink contribution to $\hat{S}_{yy}(q,\omega)$ with the aid of Eq. (120), by taking the renormalization of the kink energies into account. In fact, for finite T, not only the anharmonic contributions to $S_{yy}(q,\omega)$ become important, but also the kink energy is reduced from its bare value according to[21]

$$E_k(T) = E_k^0 - \tfrac{1}{2} k_B T - \tfrac{1}{2} k_B T \ln\left[8 \frac{E_k^0}{k_B T}\right] \ . \tag{159}$$

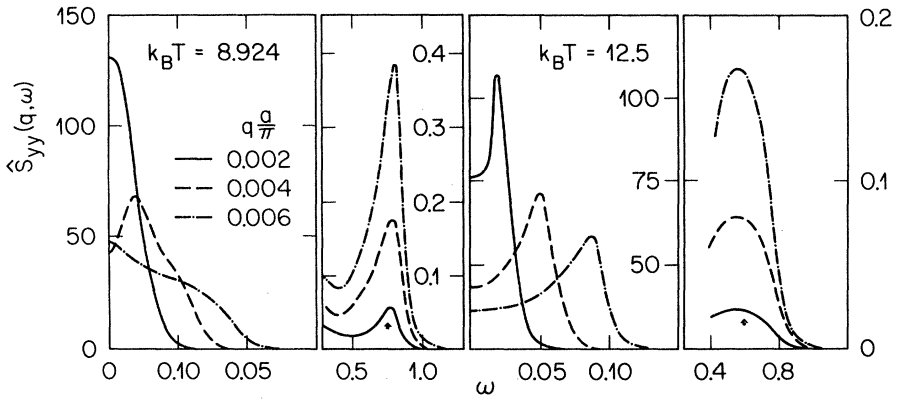

FIG. 5. $\hat{S}_{yy}(q,\omega)$ of the sG chain at some fixed q values. The arrow marks the peak position of the optic-phonon branch predicted by the high-frequency approximation [Eqs. (62) and (69)]. (From T. Schneider and E. Stoll, Springer Series in Solid-State Sciences 23, 1981, p. 82.)

To account for this effect, we replaced the bare-kink rest energy in Eq. (120) by the estimate resulting from Eq. (159). A comparison between the renormalized kink-gas predictions and the MD results is given in Fig. 7. In view of the fact that there is no adjustable parameter, the agreement is most remarkable. From Fig. 7 it is also seen that the renormalization of the kink energy is an important effect, to account for the splitting of the resonance at $k_BT=12.5$. It should be kept in mind, however, that in the ideal kink-gas picture used here, lifetime effects have been neglected. The slight discrepancies seen in Fig. 7 must be attributed to these effects. They are most clearly seen in the scaling properties of $S_{yy}(q,\omega)$. In fact, assuming that $S_{yy}(q,\omega)$ is a homogeneous function of the form[12]

$$\lambda S_{yy}(q,\omega)=\lambda^{-a-b}S_{yy}(\lambda^{-a}q,\lambda^{-b}\omega) \ , \tag{160}$$

it follows from the ideal kink-gas expression [Eq. (120)], that

$$a=1, \quad b=1 \ , \tag{161}$$

while MD leads to the estimate

$$a=1, \quad b=\tfrac{3}{2} \ , \tag{162}$$

where $a=1$ is given by the q^{-2} behavior of the static correlation function $S_{yy}(q,t=0)$. For a more detailed discussion of this scaling property and its implications for the long-time behavior, we refer to Ref. 12. Nevertheless, the remarkable agreement seen in Fig. 7 strongly suggests that the low-frequency resonance must be attributed to kinks.

This interpretation can be further substantiated by considering the time evolution of kink patterns. For this purpose, we used a π detector, marking particles passing the maximum of the single-site potential by a dot. In Fig. 8 we show the time evolution of the π signals for $k_BT=12.5$. Important in this context are the line patterns demonstrating the occurrence of propagating kinks. The velocity is distributed around

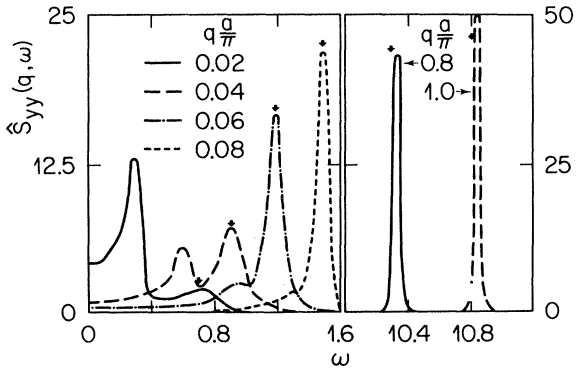

FIG. 6. $\hat{S}_{yy}(q,\omega)$ of the sG chain at some fixed q values for $k_BT=12.5$. The arrow marks the peak position of the optic-phonon branch predicted by the high-frequency approximation [Eqs. (62) and (69)].

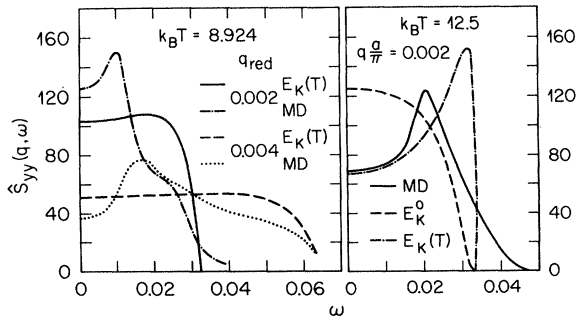

FIG. 7. $\hat{S}_{yy}(q,\omega)$ comparison of MD results and the ideal kink-gas prediction [Eq. (120)] with renormalized kink energy [Eq. (159)].

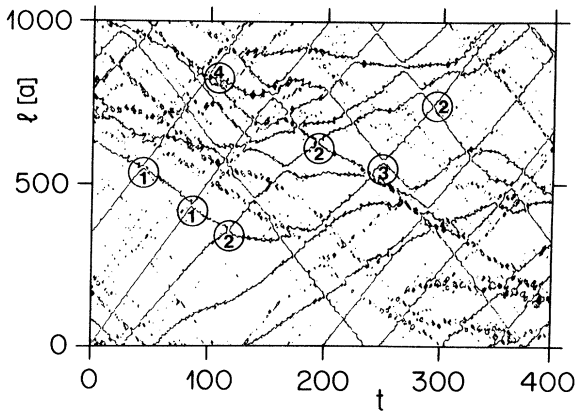

FIG. 8. Time evolution of the π signals at $k_BT=12.5$. The marked collisions are discussed in the text. ① kink-kink collision ($0\text{-}2\pi \rightarrow 2\pi\text{-}4\pi$), ② kink-antikink collision, ③ breather creation, ④ breather decay. (From T. Schneider and E. Stoll, Springer Series in Solid-State Sciences 23, 1981, p. 84.)

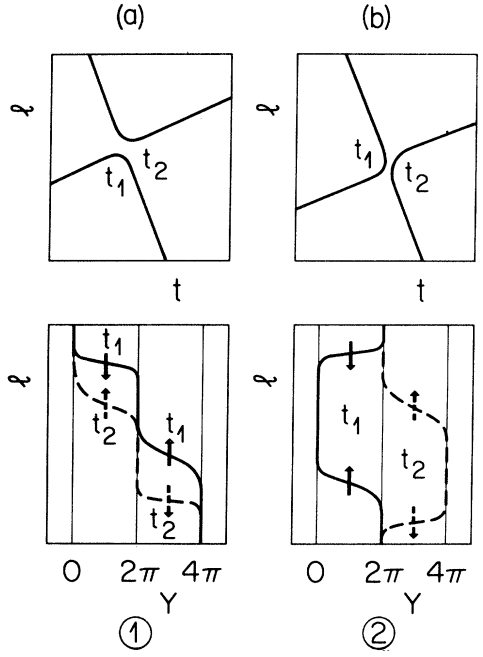

FIG. 9. Schematic sketch of the trajectories and the displacement patterns. (a) $0\text{-}2\pi \rightarrow 2\pi\text{-}4\pi$ and a kink-kink collision; (b) kink-antikink collision.

$V_k = \pm 4a$. This value agrees with the group velocity derived from the peak positions of the low-frequency resonance in Fig. 5. Other important features are the collisions allowing kinks and antikinks to be identified. According to Figs. 9 and 10 the event marked by ① corresponds to a collision of a $0\text{-}2\pi$ kink with a $2\pi\text{-}4\pi$ kink, propagating with opposite velocity. With the aid of Figs. 9 and 10, the event at $t=110$ and marked by ② in Fig. 8 is identified to be a kink-antikink collision. It is important to emphasize that the kink-kink and kink-antikink collisions are associated only with a phase shift (small shift of the trajectory) without changing the velocity. As a consequence, these collisions are not dissipative.

So far, we have concentrated on the kink features in Fig. 8, characterized by the line patterns. Closer examination also reveals the occurrence of bubbles, which must be attributed to large-amplitude breathers. The breather solution of the sG equation [Eqs. (6) and (7)] reads[22]

$$\phi_B(y,t)=4\tan^{-1}\left\{\left[\left(\frac{\Omega_0^2}{\Omega^2}-1\right)^{1/2}\sin\frac{\Omega(t-vy/c_0^2)}{(1-v^2/c_0^2)^{1/2}}\right]\operatorname{sech}\left[\left(\frac{\omega_0}{c_0}\right)\frac{(y-vt)(1-\Omega^2/\Omega_0^2)^{1/2}}{(1-v^2/c_0^2)^{1/2}}\right]\right\} \tag{163}$$

with rest energy

$$E_B=2E_k^0(1-\Omega^2/\Omega_0^2)^{1/2},\quad \Omega_0^2=\omega_0^2\ . \tag{164}$$

Note that Ω, the oscillation frequency of the breather, lies below Ω_0. For $\Omega=0$, the rest energy E_B is equal to that of a kink plus antikink; the breather amplitude approaches 2π and the breather extent approaches twice that of the kink. For $\Omega \rightarrow \Omega_0$, the breather is very extended, whereas its envelope amplitude and E_B approach zero. Since the breather activation energy can be very small, and even almost zero, we can expect the breather to be important even for $k_BT \ll E_k^0$.

From Eq. (163), it is seen that a breather can produce two separated π signals at a time. As time evolves, the amplitude of the breather changes due to the internal oscillation. Accordingly, the two signals collapse if the amplitude becomes π, and will disappear for smaller amplitudes. The resulting bubble will again appear, however, if the amplitude becomes equal to $-\pi$. Figure 8 clearly demonstrates the occurrence of such large-amplitude breathers, and reveals their importance in the decay and creation channels for kinks. In fact, the kink-antikink collision marked by ③ leads to a breather creation, and ④ marks the decay of a breather in a kink and antikink. These collisions limit the lifetime of the kinks and are further illustrated in Fig. 11. These lifetime effects are not taken into account in the ideal kink-gas phenomenology, and partially explain the slight discrepancies in Fig. 7. A more quantitative conse-

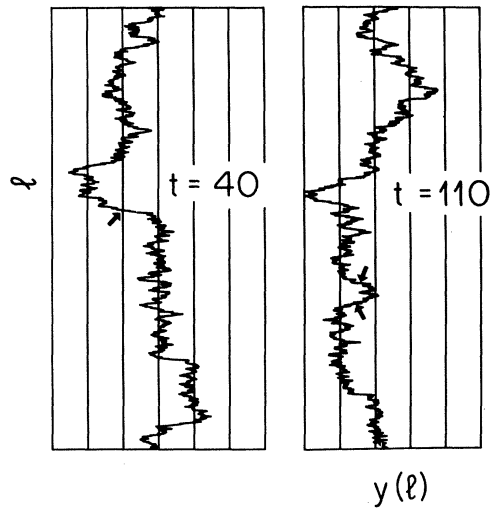

FIG. 10. Instantaneous displacement patterns of the sG chain. The kink-kink collision ($t=40$) and the kink-antikink collision ($t=110$) are marked by arrows ($k_BT=12.5$).

quence has been found in the context of the scaling properties of $\hat{S}_{yy}(q,\omega)$ revealing that lifetime effects lead to an increase of the exponent b [Eq. (162)].

From these results, including the comparison with the ideal kink-gas picture and the signal patterns of the π detector, one is naturally led to the conclusion

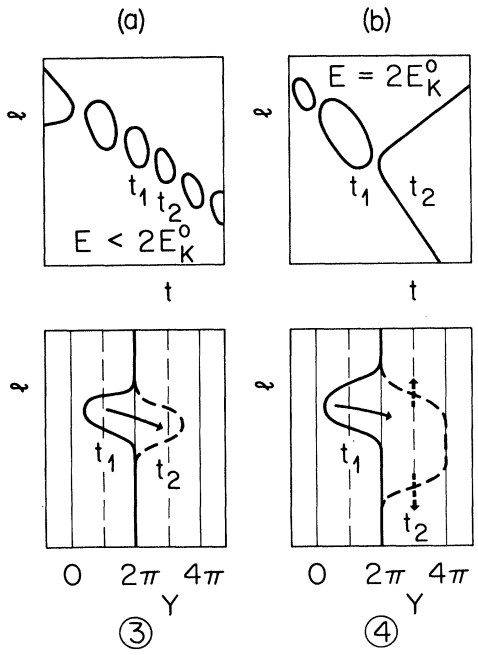

FIG. 11. Schematic sketch of the trajectories and the displacement patterns in (a) kink-antikink collision resulting in the creation of a breather; (b) decay of a breather in a kink-antikink pair.

that the low-frequency resonance in $\hat{S}_{yy}(q,\omega)$ (Fig. 5) is due to kinks. The strength of this resonance depends sensitively on q, as expected from Eq. (120), or more precisely, from the scaling property [Eqs. (160) and (162)]

$$\hat{S}_{yy}(q,\omega)=q^{-b}S_{yy}(1,\omega/q^b) \quad . \tag{165}$$

This interpretation of the low-frequency resonance in terms of a kink excitation branch is also consistent with the temperature dependence of the static form factor $S_{yy}(q,t=0)$ for $T\to 0$.

For higher temperatures ($k_BT>12.5$), however, the ideal kink-gas picture and the renormalization concept of the kink energy breakdown. In fact, in the ideal kink-gas picture, we assumed $\beta E_k^0 >> 1$, and the WKB approximation on which the kink-energy renormalization relies, only holds for $k_BT << 29.22$ [Eq. (158)]. Moreover, the transfer-integral results for $S_{yy}(q)$ clearly indicated that already for $k_BT \gtrsim 20.86$, the high-temperature expression (97) for $S_{yy}(q,t=0)$ holds quite well. As a consequence, kinks are no longer expected to play a role and the high-temperature approximations [Eqs. (62) and (65)] are expected to apply, predicting a resonance at $\omega=\pm\omega_T(q)$ for small q and for large q, close to $\omega=\pm\omega_A(q)$ [Eq. (69)]. According to Eqs. (50) and (97), ω_T^2 is given by

$$\omega_T^2=2\frac{c_0^2}{a^2}(1-\cos qa) \quad . \tag{166}$$

For intermediate q values, one expects a crossover between the low- and high-frequency behaviors [Eq. (96)].

To test these expectations, we now turn to the MD results for $k_BT=20.86$, shown in Figs. 12 and 13. The frequencies $\omega_A(q)$ and $\omega_T(q)$, as obtained from Eqs. (69), (166), and Table IX, are marked by ar-

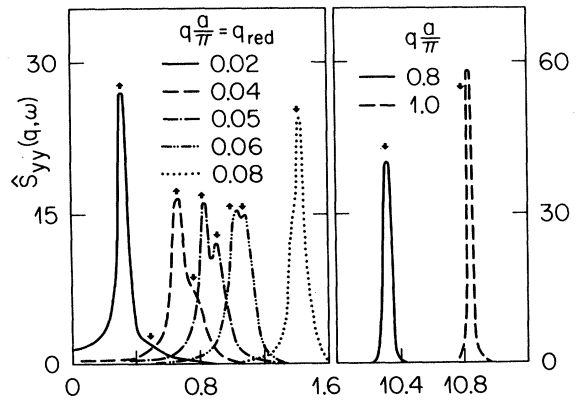

FIG. 12. $\hat{S}_{yy}(q,\omega)$ for fixed intermediate and large q values at $k_BT=20.86$. $\downarrow\omega_A(q)$ [Eq. (69) and Table IX]; $\uparrow\omega_T(q)$ [Eq. (166)].

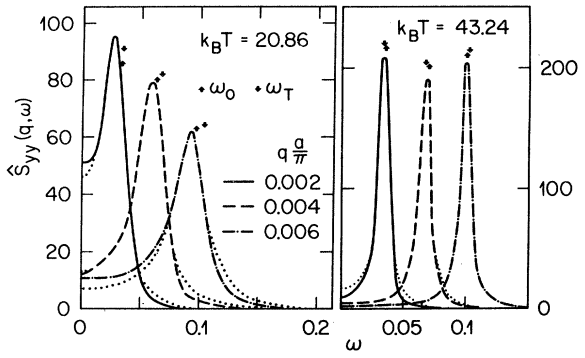

FIG. 13. $\hat{S}_{yy}(q,\omega)$ for small fixed q values. For comparison, we included a Lorentzian profile (dotted) resulting from a fit to the peak position and peak height. The parameters are listed in Table X.

rows. For large wave numbers, the peak positions agree very well with ω_A. The split peaks at about $qa/\pi = 0.04$–0.08, however, reveal a crossover from the high-frequency [Eq. (62)] to the low-frequency regime [Eq. (65)]. In fact, for smaller wave numbers, the peak positions are very close to ω_T, as shown in Fig. 13. For comparison, we also included the Lorentzian profile [Eq. (65)], resulting from a fit to the peak position ω_0 and the peak height of the MD results. The corresponding results for $k_BT = 43.244$ are shown in Fig. 13. The peak positions and the fitted half-width are listed in Table X, revealing that Γ_l decreases with increasing temperature. This behavior simply reflects the fact that the periodic single-site potential becomes gradually irrelevant in the limit $T \to \infty$, so that the system tends to a harmonic chain, with infinitely long-lived phonons.

From the excellent agreement between the molecular-dynamics results and the low- and high-frequency approximations, we then conclude that the excitation spectrum for $k_BT \geq 20.86$, seen in $\hat{S}_{yy}(q,\omega)$, can be fully understood in terms of interacting phonons and the crossover from a high- to a low-frequency regime. For small wave vectors, the low-frequency approximation is adequate, while for large wave numbers, the high-frequency approximation holds.

Finally, we revert to the weak high-frequency resonance in the low-temperature regime, as seen in Figs. 5 and 6. According to the high-frequency approximation, such a resonance is expected to occur close to $\omega_A(q)$ [Eqs. (62) and (69)]. These frequencies, as obtained from the gaps $\omega_A(q=0)$ listed in Table IX are marked by arrows. The excellent agreement between $\omega_A(q)$ and the MD results clearly indicates that this excitation branch must be attributed to the optic-phonon branch with dispersion $\omega_A = \omega_A(q)$. From Fig. 6, it is also seen that the optic-phonon resonance dominates the excitation spectrum of $\hat{S}_{yy}(q,\omega)$, except for very small wave numbers. Here the spectrum is exhausted by the kinks, that is to say, as a function of the wave number and at low temperatures, we have a crossover from a kink to an optic-phonon-dominated spectrum. This crossover is also illustrated in Fig. 14, showing the dispersion laws resulting from the peak positions observed in $\hat{S}_{yy}(q,\omega)$ at $k_BT = 12.5$. Except for very small q values, where the kink resonance dominates, the spectrum can be fully understood in terms of the optic-phonon branch.

To summarize, we have found clear evidence for a kink excitation branch for $k_BT \lesssim 12.5$, exhausting the spectrum for small q and ω values. With increasing wave number, a crossover occurs to an optic-

TABLE X. Parameters resulting from fitting a Lorentzian profile [Eq. (65)] to the MD peaks shown in Fig. 13 in terms of the peak position ω_0 and the peak height. For comparison, we included the corresponding values of ω_T [Eq. (166)].

qa/π	ω_T	ω_0	Γ_l	ω_0	Γ_l
0.002	0.034	0.033	0.024	0.035	0.010
0.004	0.068	0.063	0.026	0.070	0.011
0.006	0.102	0.096	0.033	0.100	0.010
k_BT		20.86		43.244	

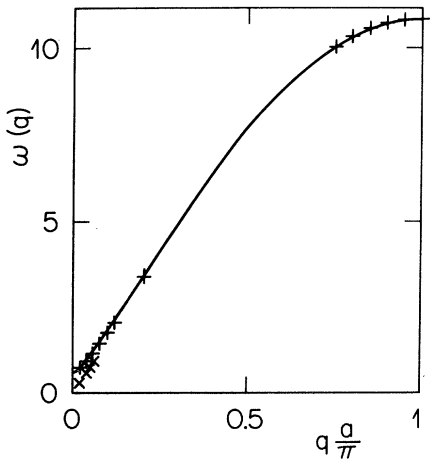

FIG. 14. Dispersion laws resulting from a fit to the peak positions observed in $\hat{S}_{yy}(q,\omega)$ at $k_BT = 12.5$. The full line corresponds to the estimate $\omega_A(q)$ [Eq. (69)] for the optic-phonon branch, as predicted by the high-frequency approximation [Eq. (62)].

phonon-dominated spectrum. The ideal kink-gas approximation, with renormalized kink energy turned out to be a surprisingly good approximation for the kink resonance. For $k_B T \gtrsim 20.86$, however, the kinks were found to be irrelevant, and the spectrum was understood in terms of the low- and high-frequency approximations, appropriate for a weakly interacting phonon gas.

B. $\hat{S}_{ss}(q,\omega)$

The dynamic form factors $S_{ss}(q,\omega)$ and $S_{yy}(q,\omega)$ are closely related, because (Table VI)

$$\omega_0^4 S_{ss}(q,\omega) = S_{yy}(q,\omega) \times \left[\omega^2 - \frac{2c_0^2}{a^2}(1-\cos qa)\right]^2 . \quad (167)$$

For

$$qa << 1, \quad \omega << c_0 q ,$$

Eq. (167) reduces to

$$\omega_0^4 S_{ss}(q,\omega) = S_{yy}(q,\omega)(c_0 q)^4 , \quad (168)$$

and for

$$\omega >> c_0 q , \quad (169)$$

$$\omega_0^4 S_{ss}(q,\omega) = S_{yy}(q,\omega)\omega^4 . \quad (170)$$

Recalling then that at low temperatures and small q values, we see that $S_{yy}(q,\omega)$ is dominated by the kink excitation branch, occurring close to $\omega = 0$ (Fig. 5), it follows from Eq. (168) that this resonance will be very weak in $\hat{S}_{ss}(q,\omega)$, due to the q^4 prefactor. This fact is nicely illustrated in Fig. 15, revealing very weak kink resonances for small q values. As expected from Eq. (168), its strength increases with q.

For large frequencies, $\hat{S}_{yy}(q,\omega)$ exhibits a weak phonon resonance (Figs. 5 and 6). According to Eq. (170), this peak will not be suppressed in $S_{ss}(q,\omega)$ because $\omega_A \approx 1$ (Table IX). Due to the ω^4 prefactor, the peak position will be shifted, however, to slightly higher frequencies. These expectations are confirmed by the MD results shown in Fig. 15.

To summarize, for small wave numbers, $\hat{S}_{ss}(q,\omega)$ is dominated by the phonon peak. Due to the ω^4 prefactor, its position is slightly shifted to higher frequencies. The kink excitation branch, occurring at small frequencies and low temperatures, is suppressed due to the q^4 prefactor, but its strength increases with q. In the high-temperature regime ($k_B T \gtrsim 20.84$), essentially the same reasoning is found to apply, but with the kink resonance replaced by the low-frequency phonon resonance (ω_T).

C. $\hat{S}_{cc}(q,\omega)$

This dynamic form factor is of particular interest, because the cosines of the displacements might be particularly sensitive to breathers [Eq. (163)] with an amplitude of about π. To substantiate this conjecture, it is important to recognize that the breather amplitude [Eq. (163)] can adopt both signs. Accordingly, $\cos y_l - \langle \cos y_l \rangle$ is maximum for $y_l \approx \pm n\pi$. This fluctuation is small, however, for kinks and phonons, because $y_l \approx \pm 2\pi n$, with the exception of the kink wall. We expect, therefore, that $S_{cc}(q,\omega)$ will be particularly sensitive to large-amplitude breathers.[10] The occurrence of such breathers is clearly demonstrated in Fig. 8 in terms of the bubbles. On the basis of these arguments, for small q values we expect two resonances in $\hat{S}_{cc}(q,\omega)$. A low-frequency resonance, associated with the propagating breather envelope, and a high-frequency peak due to the internal breather oscillations. From

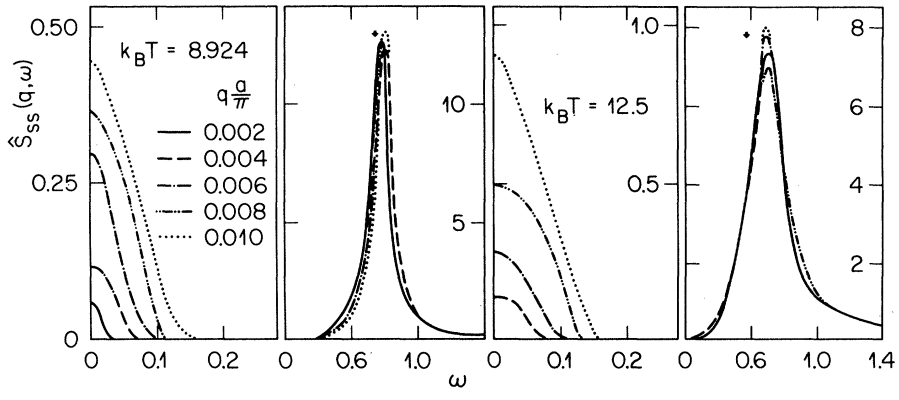

FIG. 15. $S_{ss}(q,\omega)$ for some fixed q values. The arrow marks $\omega_A(q)$.

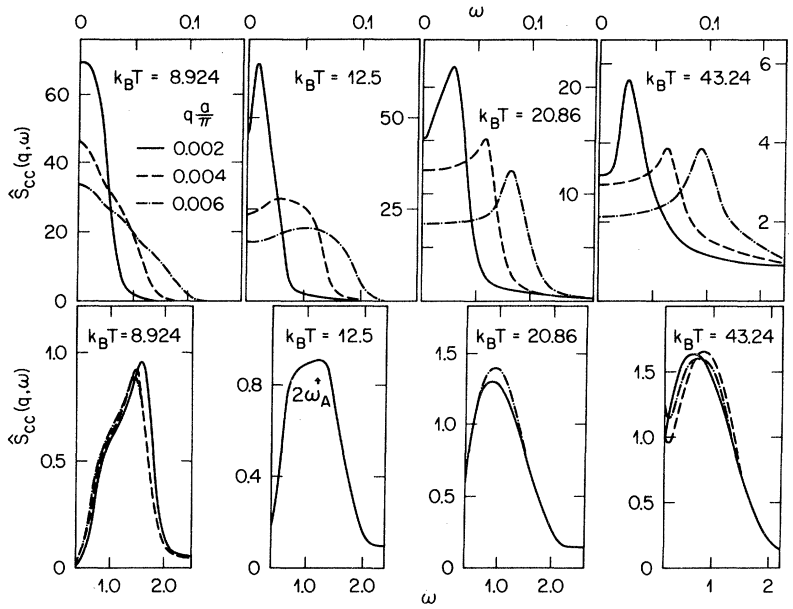

FIG. 16. $\hat{S}_{cc}(q,\omega)$ at some fixed q values. (From T. Schneider and E. Stoll, Springer Series in Solid-State Sciences 23, 1981, p. 82.)

Fig. 8, it is seen that the breather velocities v_B are distributed around $v_B^0 \approx \pm 1.6a$ at $k_BT = 12.5$. The double-peak structure of the breather-velocity distribution may be understood in terms of the relativistic Boltzmann-gas picture. Accordingly, we expect the breather-envelope resonance to split with increasing temperature. Such features are indeed observed in the molecular-dynamics results shown in Fig. 16, including a cutoff at $\omega = 2\Omega_0 = 2$ [Eq. (164)] of the high-frequency resonance.

On the other hand, one expects that the low-temperature behavior of $S_{cc}(q,\omega)$ can be understood in terms of two-phonon processes [Eq. (88)]. For this reason, we also calculated $\hat{S}_{cc}(q,\omega)$ on the basis of Eq. (88). The results are shown in Fig. 17 for $T \to 0$. Comparing these results with Fig. 16, it is seen that the two-phonon approximation accounts almost quantitatively for the low-frequency resonance. Significant discrepancies are present for the high-frequency peak. In fact, the two-phonon sum process has a cutoff at $\omega \lesssim 2$, while the MD results agree much better with the breather cutoff at $\omega \gtrsim 2$. In this context, it should be kept in mind, however, that the two-phonon approximation for $S_{cc}(q,\omega)$ at best is valid only for $T \to 0$. For $k_BT = 8.924$, not only the higher-order normal phonon processes, but also umklapp processes and lifetime effects become important. The higher-order phonon processes will shift the high-frequency resonance to lower frequencies with increasing temperature, and will give rise to additional high-frequency peaks around $\omega = 4\omega_A(0)$, $6\omega_A(0)$, ...

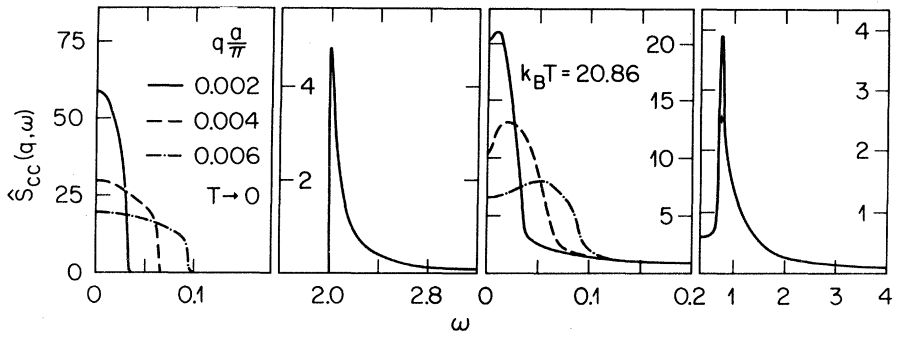

FIG. 17. Two-phonon approximation for $\hat{S}_{cc}(q,\omega)$ at some fixed q values, [Eq. (88)] for low temperatures, and evaluated with the aid of the harmonic approximation at $k_BT = 20.86$. The arrow marks $2\omega_A$ [Eq. (69)].

An additional difficulty in the interpretation of $\hat{S}_{cc}(q,\omega)$ stems from the coupling between the $\cos x_l - \langle \cos x_l \rangle$ and the energy fluctuations. That is to say, that $\hat{S}_{cc}(q,\omega)$ does have a contribution from $\hat{S}_{HH}(q,\omega)$. Because $\hat{S}_{HH}(q,\omega)$ is found to be exhausted by a low-frequency second-sound resonance, this contribution affects the low-frequency structure of $\hat{S}_{cc}(q,\omega)$ only. As noted above, this part of the spectrum is quite well described by the two-phonon approximation, becoming exact in the limit $T \to 0$.

In view of this, an unambiguous identification of the low- and high-frequency resonances appearing in $S_{cc}(q,\omega)$ at $k_B T = 8.924$ and 12.5 is not possible (Fig. 16). The dominant contribution must be attributed to two- and higher-phonon processes which themselves may form breathers. This possibility is clearly supported by the presence of breather features, seen by the π detector (Fig. 8).

Let us then turn to the high-temperature regime, where anharmonic perturbation theory is gradually becoming exact. The molecular-dynamics results for $k_B T = 20.86$ and 43.244 are shown in Fig. 16. Even though the overall features are qualitatively similar to those found in the low-temperature regime, the interpretation must be quite different. In fact, for $k_B T \geq 20.86$, the excitation spectrum seen in $\hat{S}_{yy}(q,\omega)$ could be fully understood in terms of a weakly interacting phonon gas. Clearly, the associated oscillations will have large amplitudes, so that $\cos y_l$ can no longer be expanded, even though $y_l(t)$ evolves almost according to the harmonic approximation [Eq. (83)]. On this basis, we evaluated $S_{cc}(q,\omega)$ numerically, with the aid of Eq. (83). The results are shown in Fig. 17 for $k_B T = 20.86$. Comparison with the MD results given in Fig. 16 reveals that the low-frequency resonance is well described by the harmonic contributions. The high-frequency resonance seen in MD, is however, much broader. Finally, we turn to the integrated intensity of the low-frequency resonance (cp), defined by

$$\frac{1}{2\pi}\int_{\rm cp} \hat{S}_{cc}(q=0,\omega)\,d\omega \ , \tag{171}$$

because the main contribution is expected to arise from the two-phonon difference process at low temperatures, and from the harmonic contributions for $T \to \infty$. A comparison between these predictions and the MD results is given in Fig. 18, revealing that the approximate treatments describe surprisingly well, the observed temperature dependence.

To summarize, the low-frequency peak in $\hat{S}_{cc}(q,\omega)$ can be explained in terms of the two-phonon difference processes at low temperature, and by means of the harmonic approximation at high temperatures. There is no clear evidence to attribute part of the low-fequency peak to the breather envelope. The high-frequency peak, however, is not well accounted for by these approximations, while the breather interpretation is consistent with the high-frequency cutoff observed.

D. $\hat{S}_{HH}(q,\omega)$

Due to energy conservation, $S_{HH}(q,\omega)$ is expected to exhibit a resonance associated with a hydrodynamic mode (Sec. IV). At low temperature, where also the field momentum will be nearly conserved, heat diffusion will be underdamped and propagate in terms of second sound. Assuming well-defined second sound, we expect a resonance close to

$$\omega_{ss}^2(q) = q^2 \frac{c_0^4 D}{a T c_V} 2 \frac{1}{N} \times \sum_{q'} (1-\cos q' a)\,\langle |y(q')|^2 \rangle \ . \tag{172}$$

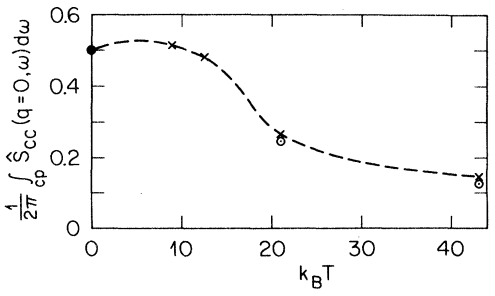

FIG. 18. Temperature dependence of the integrated intensity of the low-frequency resonance in $\hat{S}_{cc}(q,\omega)$. For comparison, we included ⊙: harmonic approximation, ●: two-phonon difference process [Eq. (88)], ×: MD.

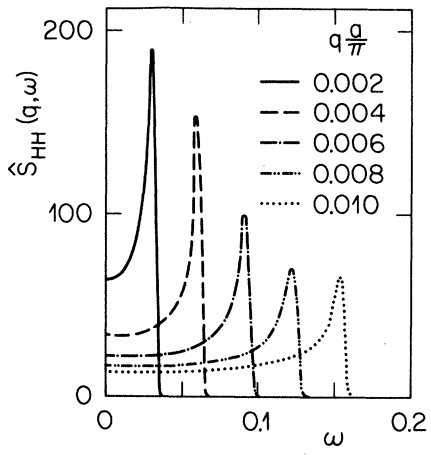

FIG. 19. $\hat{S}_{HH}(q,\omega)$ as obtained with the aid of the two-phonon approximation Eq. (87) for $k_B T = 8.924$.

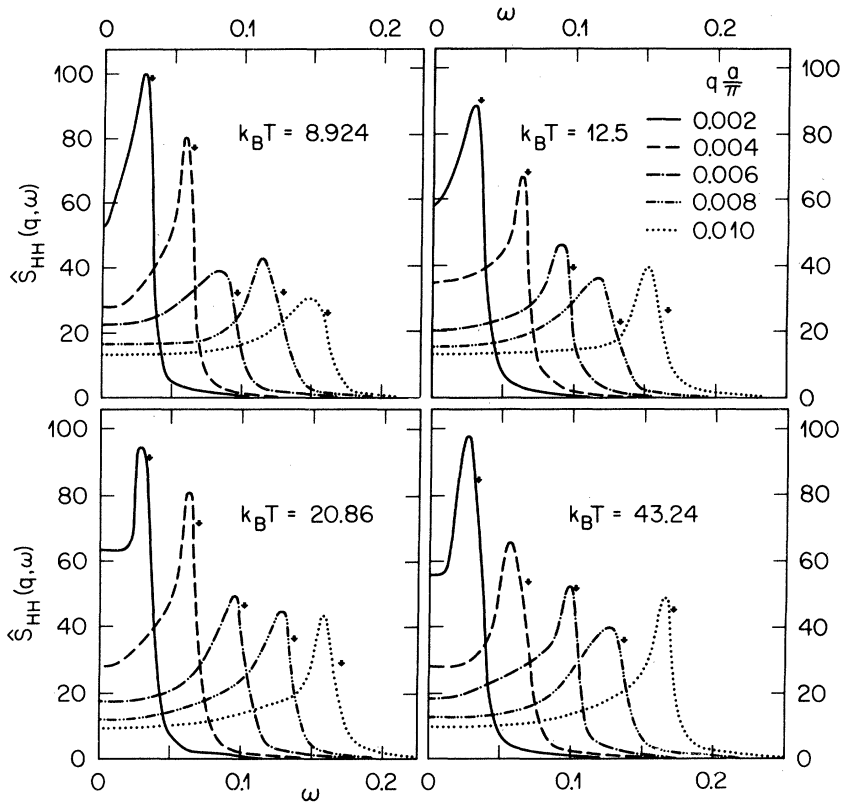

FIG. 20. $\hat{S}_{HH}(q,\omega)$ for some fixed q values. Arrows mark the second-sound frequency estimate [Eq. (172), Table IX].

Here we replaced q'^2a^2 in Eq. (79) by $2(1-\cos q'a)$. The resulting estimates for ω_{ss} are listed in Table IX, where the specific heat c_V and the last term in Eq. (172) have been calculated with the aid of the transfer-integral technique. According to phonon hydrodynamics, the resonance should be a Lorentzian, approximately given by Eq. (81), where the lifetime effects are taken into account. Such lifetime effects are not included in the two-phonon approximation: As a consequence, the difference phonon peak is not in general, Lorentzian, as illustrated in Fig. 19 by the rather sharp high-frequency cutoff.

The molecular-dynamics results for $\hat{S}_{HH}(q,\omega)$ are shown in Fig. 20. For comparison, we also included the peak positions resulting from Eq. (172) and Table IX. They are marked by arrows. Obviously, the peak positions observed agree well with the estimates, and depend linearly on the wave number. The slight overestimate by the peak positions by ω_{ss} can be attributed to neglect of the imaginary part of the memory function, leading to a shift. More important is the fact that the resonance shapes are nearly Lorentzian and differ in this respect from the shape of the low-frequency peak in the two-phonon approximation (Fig. 19). Owing to the nearly Lorentzian shape of the resonance and the good agreement between ω_{ss} and the observed peak positions, we conclude that the resonances shown in Fig. 20 are due to second sound. Given this identification, it is remarkable that second sound persists in being well defined over an extremely broad temperature range. In fact, from $k_BT=8.924$ up to 43.244, there is no significant change in the shape of $\hat{S}_{HH}(q,\omega)$. This feature reveals that the sG chain does have an exceptionally large temperature window where well-defined second sound exists. This property is consistent with the fact that in the high-temperature regime, the interactions of the sG phonon become weaker with increasing temperature.

VII. MOLECULAR-DYNAMICS RESULTS: ϕ^4 CHAIN

In this section, we shall present and discuss some dynamic form factors of the ϕ^4 chain, which, in its d-dimensional formulation, represents a useful model for distortive phase transitions. In the terminology of critical phenomena, the model belongs to the Ising universality class. The choice of the model parameters in the Hamiltonian [Eqs. (1) and (3)] is summarized in Table XI, with units defined by Eq. (127). For dimensions $d>1$, the system undergoes a ferrodistortive phase transition at $T=T_c$ provided the single-site potential has a double-well structure,

TABLE XI. Model parameters of the ϕ^4 chain.

Model	$\Delta=\omega_0^2$	$\Delta/2c_0^2$	$B=b\omega_0^2$	b	E_k^0
I	2	2	$\frac{1}{3}$	$\frac{1}{6}$	5.657
II	0.125	0.125	$\frac{1}{3}$	$\frac{8}{3}$	0.088
III	0.05	0.05	$\frac{1}{3}$	$\frac{20}{3}$	0.0224

which is guaranteed for

$$\Delta > 0 \ . \tag{173}$$

Here, we consider $d=1$ only, where the order parameter

$$\langle y_l \rangle_{T=0}^2 = y_l^2 = \frac{\Delta}{B} \tag{174}$$

is nonvanishing at $T=0$ only. Thus, $T=0$ may be viewed as the transition temperature.

The system is a lattice dynamic realization of a model for ferrodistortive phase transitions, which covers the two limiting classes of real systems, the order-disorder and the displacive regimes. By approaching the displacive limit ($\Delta/2c_0^2=0$), the wells of the single-site potential become shallow. This regime corresponds to the strong coupling limit. In the order-disorder limit ($\Delta/2c_0^2 >> 1$), the potential wells are very deep and the partition function becomes equivalent to that of the Ising model. Adopting this terminology, models II and III (Table XI) then belong to the displacive regime, whereas model I is an order-disorder system. Here, we shall concentrate on model III but to explore the Δ dependence, locating a system on the displacive-order-disorder scale, we shall also consider models I and II, to elucidate possible differences in the excitation spectrum. Particular emphasis will be placed on the Δ dependence of the relaxation time of critical slowing down,[23]

$$\tau_{yy} = \lim_{\omega \to 0} \hat{S}_{yy}(q=0,\omega) \ , \tag{175}$$

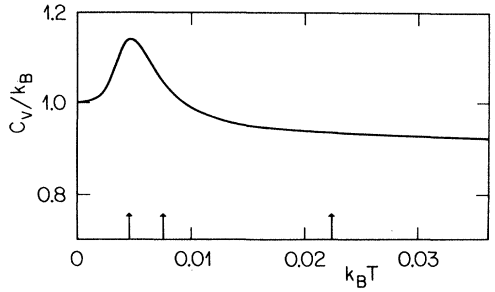

FIG. 21. Temperature dependence of the specific heat for model III as obtained from a numerical solution of the transfer-integral equation. Arrows mark the temperatures for which MD results will be presented.

which is expected to diverge by approaching $T=0$ [Eq. (140)].

To identify the low-, intermediate-, and high-temperature regimes, in Fig. 21 we show the temperature dependence of the specific heat for model III. The particular temperatures for which MD results will be presented are marked by arrows.

A. $\hat{S}_{yy}(q,\omega)$

According to the ideal kink-gas picture, for small q and ω, we expect a resonance due to the kinks. It will be a peak centered around zero frequency (Fig. 3). In contrast to the sG case, $\hat{S}_{yy}(q,\omega)$ will be well behaved for $q \to 0$, because the particles are localized in the double well. In fact, the system can be visualized as an elastic linear chain subjected to a double-well potential, where $v(y_l) \to \infty$ for $y_l \to \pm\infty$.

Numerical results for $\hat{S}_{yy}(q,\omega)$ are shown in Fig. 22 for model III at $k_BT=0.00448$, 0.00747, 0.0224, and 0.224, respectively. For comparison, in Fig. 23 we included the corresponding predictions of the ideal kink-gas picture. These results have been obtained by Fourier transforming Eq. (132) numerically.

Figure 22 clearly reveals that for small wave numbers, the spectrum is exhausted by a low-

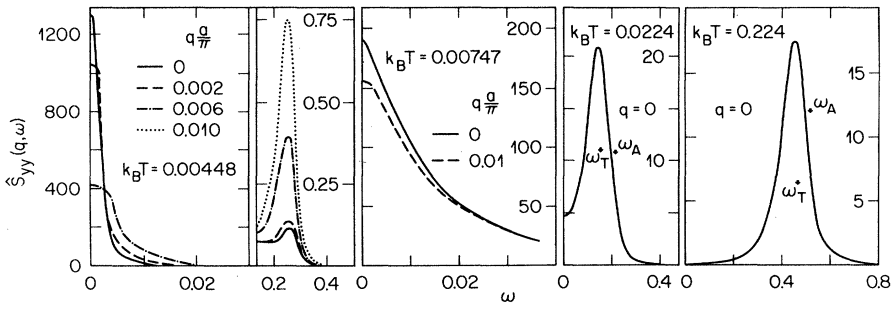

FIG. 22. $\hat{S}_{yy}(q,\omega)$ at some fixed q values for model III. (From T. Schneider and E. Stoll, Springer Series in Solid-State Sciences 23, 1981, p. 82.)

frequency resonance. Its strength and q dependence agree reasonably well with the peak predicted by the ideal kink-gas picture (Fig. 23), with unrenormalized kink energy. Inclusion of renormalization effects [$E_k^0 \rightarrow E_k(T)$] leads to a considerably worse agreement. Accordingly, the underestimate of the peak height, and the overestimate of the half-width must be attributed to lifetime effects. Nevertheless, the reasonable agreement, as obtained without any adjustable parameter, clearly indicates that the low-frequency excitation branch seen in Fig. 22 must be attributed to the kinks. Similar agreement is obtained at $k_BT=0.00747$ (Fig. 22), so that the kink-gas picture rather quantitatively describes the relative temperature dependence of the peak height, which is seen to decrease with increasing temperature, whereas the high-frequency resonance becomes stronger. In fact, at $k_BT=0.224$ and higher temperatures, the kink excitation branch is no longer visible (Fig. 22). The disappearance of the kink branch also occurs at low temperatures with increasing wave number (Fig. 22). With the exception of small q, the low-temperature excitation spectrum is seen to be exhausted by the high-frequency resonance. Its position agrees well with the marked frequency ω_A corresponding to an optic-phonon branch predicted by the high-frequency approximation [Eq. (62) and Table V], yielding

$$\omega_A^2=-\Delta+3B\langle y_l^2\rangle+\frac{2c_0^2}{a^2}(1-\cos qa) \ . \quad (176)$$

Transfer-integral estimates for $\langle y_l^2\rangle$ are listed in Table XII. Accordingly, we attribute the high-frequency resonance seen in Fig. 22 to the optic-phonon branch. The temperature dependence of the gap $\omega(q=0)$ shown in Fig. 24 reveals, however, considerable deviations from the high-frequency estimate $\omega_A(q=0)$ for $k_BT>0.00747$. This discrepancy is also illustrated in Fig. 22. According to the temperature dependence of the specific heat (Fig. 21), $k_BT=0.00747$ exceeds the location of the maximum and belongs, therefore, to the high-temperature regime, where the low-frequency approximation [Eq. (65)] predicting a resonance close to [Eq. (50)]

$$\omega_T^2(q)=\frac{k_BT}{DaS_{yy}(q,t=0)} \ , \quad (177)$$

is more appropriate.

From Figs. 22 and 24, it is seen that the ω_T estimates, as obtained with the aid of Table XII, are in excellent agreement with the MD data for $k_BT>0.00747$. Figure 24 also reveals that the softening of the gap of the optic-phonon branch is incomplete, because it reaches its minimum close to $k_BT=0.01$.

Interpretation of the low-frequency resonance, occurring at low temperatures and small values of q and ω (Fig. 22), can be further clarified by considering the time evolution of the displacement patterns. For this purpose, we used a sign detector. It marks particles with positive displacement by a black dot, and particles with a negative displacement are not shown. Propagating kinks will then be represented by a line separating black and white regions. Figure 25 shows the time evolution of the sign signals for $k_BT=0.00448$ and model III. The occurrence of line patterns clearly demonstrates the presence of propagating kinks. The propagation properties are seen to be distinctly different from those of the sG kinks (Fig. 8). In fact, Fig. 25 reveals that there are a number of events where ϕ^4 kinks reverse their velo-

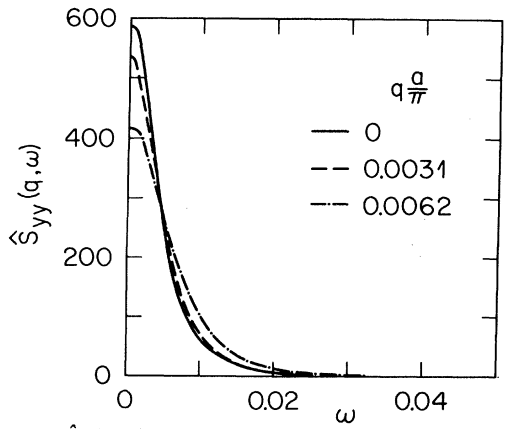

FIG. 23. $\hat{S}_{yy}(q,\omega)$ as obtained from the ideal kink-gas expression Eq. (132) for model III and $k_BT=0.00448$.

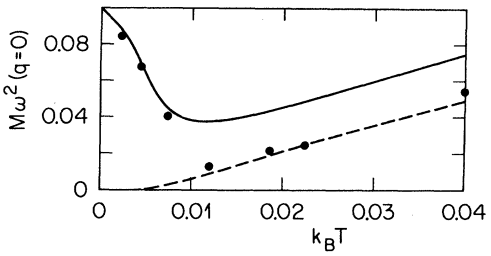

FIG. 24. Temperature dependence of the gap of the optic-phonon branch. ● MD, —— $\omega_A^2(0)$ [Eq. (176)], – – – $\omega_T^2(0)$ [Eq. (177)].

TABLE XII. Transfer-integral estimates for $\langle y_l^2\rangle$ and $S_{yy}(q=0,\ t=0)$ and the second-sound frequency [Eq. (172)] for model III.

k_BT	E_k^0/k_BT	$\langle y_l^2\rangle$	$S_{yy}(q=0,\ t=0)$	$\omega_{ss}(q=0.002a/\pi)$
0.00448	5	0.121	10.14	0.0038
0.00747	3	0.095	2.95	0.0041
0.0224	1	0.099	0.91	0.0043
0.224	10	0.322	1.04	0.0039

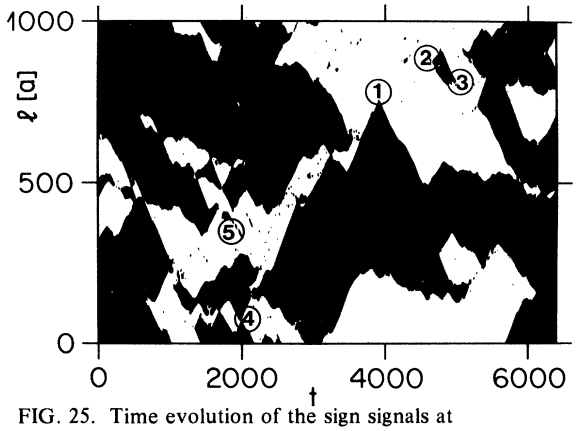

FIG. 25. Time evolution of the sign signals at $k_B T = 0.004\,48$ for model III. Particles with positive instantaneous displacement are marked by a black dot, and particles with negative displacements are not shown. The marked events denote: ① kink reverses its velocity, ② creation of a kink-antikink pair, ③ kink-antikink collision and decay into "phonons," ④ kink-antikink collision, ⑤ breatherlike features. (From T. Schneider and E. Stoll, Springer Series in Solid-State Sciences 23, 1981, p. 85.)

city. An example is the event marked by ①; the slope occurs at $t = 3920$. This feature is further illustrated in Fig. 26, showing the instantaneous displacement pattern of the chain at this time. The lower kink, which we consider as an antikink, is nearly stationary in the time interval considered here. The upper kink separates from the lower one, stops at 3920 and reverses its velocity. The chain patterns also reveal that the wall thickness of the kinks is rather small. Moreover, in Fig. 25 one can identify breatherlike patterns in terms of bubbles. It should be kept in mind, however, that the ϕ^4 system is not exactly integrable. The kink solutions are solitary waves only, and there will be no exact kink-antikink bound state, corresponding to the sG breather [Eq. (163)].

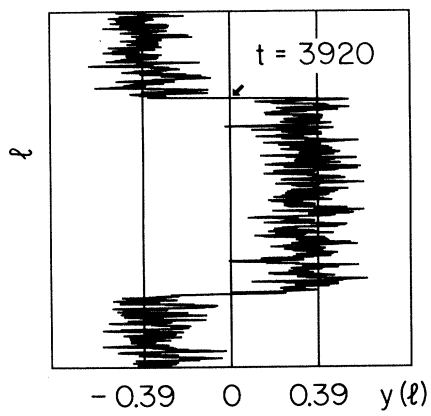

FIG. 26. Instantaneous displacement pattern at $t = 3920$ for model III at $k_B T = 0.004\,48$.

Nevertheless, Fig. 25 clearly demonstrates the existence of rather short-lived breatherlike patterns, examples being the bubbles marked by ⑤. Apart from the nearly ideal kink-kink collision ④, there are also dissipative collisions, for example ③, where a kink and antikink collide with a subsequent decay into phonons or "small-amplitude breathers." Another example is marked by ②, where a kink and antikink are created presumably from small-amplitude "breathers." Such events will affect the lifetime of the kinks. More important appears to be the processes leading to a reversal of the kink velocities. This feature is completely missing in the sG case, and leads to a nearly random-walk-type motion of the kinks (Fig. 25).

These results and discussions then lead to the conclusion that the kinks of the ϕ^4 system give rise to an excitation branch in terms of a central peak, occurring at low temperatures and small values of q and ω. It exhausts the spectrum of $\hat{S}_{yy}(q,\omega)$ at low temperatures and small wave numbers. In this regime, the ideal kink-gas approximation leads to reasonable agreement, provided the kink energy is not renormalized. Moreover, in contrast to the sG case, the relativistic effects do not play a significant role, because the motion of the kinks exhibits random-walk features. For larger wave numbers or for temperatures $k_B T > 0.007\,47$, the spectrum becomes dominated by the optic-phonon branch, undergoing a crossover from ω_A to ω_T for small q values. In the limit $T \to \infty$, which was not considered here, the system leads to independent quartic oscillators, where $S_{yy}(q,\omega)$ is given by Eq. (99).

So far, we have considered model III (Table XI) only, belonging to the displacive regime, characterized by a shallow single-site double well. To characterize the Δ and T dependence of the crucial features of the excitation spectrum, we next introduce the line[23]

$$\int_{\text{cp}} \hat{S}_{yy}(q=0,\omega)\frac{d\omega}{2\pi} = f(\Delta,T) \ , \tag{178}$$

for fixed values of B. Here, the integral extends over the kink resonance only. Because

$$\int_{-\infty}^{+\infty} \hat{S}_{yy}(q=0,\omega)\frac{d\omega}{2\pi} = 1 \ , \tag{179}$$

$f(\Delta,T)$ satisfies

$$0 \leq f(\Delta,T) \leq 1 \ . \tag{180}$$

For $f(\Delta,T)=0$, there is no kink resonance, and for $f(\Delta,T)=1$, it exhausts the spectrum. As a consequence

$$f(\Delta,T^*) = 0.5 \tag{181}$$

defines a "crossover" line where 50% of the normalized weight of $\hat{S}_{yy}(q=0,\omega)$ is in the kink resonance, and 50% in the optic-phonon resonance. Using Eqs.

(178) and (179), we evaluated

$$T^* = T^*(\Delta/2c_0^2) \tag{182}$$

numerically for the three models listed in Table XI. The results are shown in Fig. 27. Below the T^* line, $\hat{S}_{yy}(0,\omega)$ is dominated by the kink resonance, and above by the optic-phonon branch. For $\Delta \to 0$, T^* can be estimated from Eq. (139) by observing that T enters only in the combination βE_k^0. It then follows that

$$\frac{E_k^0}{T^*} = \text{const.} \tag{183}$$

When one invokes (Tables I and XI)

$$E_k^0 = 2\frac{\sqrt{2}}{3} D\omega_0 c_0 \frac{1}{b} = 2\frac{\sqrt{2}}{3} D\Delta^{3/2}\frac{c_0}{B} \ , \tag{184}$$

it then follows that

$$T^* = \text{const}\left(\frac{\Delta}{2c_0^2}\right)^{3/2} \ . \tag{185}$$

This asymptotic form is also included in Fig. 27 with the numerically estimated prefactor (const ≈ 11.3).

Figure 27 then demonstrates that, for displacive systems and $q=0$, the kink excitation branch always exhausts the excitation spectrum for sufficiently low temperature. For $\Delta \to 0$, however, this temperature region shrinks to zero, and the spectrum will be dominated for accessible temperatures by the phonon branch. For $\Delta = 0$, there is no longer a double well, and anharmonic perturbation theory becomes applicable. Here, the spectrum will be dominated by the gap of the optic-phonon branch, given by

$$\omega_A^2(0) = 3B\langle y_l^2\rangle \ , \tag{186}$$

which becomes soft, because $\langle y_l^2\rangle \to 0$ for $T \to 0$ ($\Delta = 0$). For any nonvanishing Δ, however, the kink resonance will dominate for $T \to 0$, even though the temperature interval where this happens shrinks itself to zero by approaching $T=0$. Clearly, very low temperatures are academic in any case because quantum effects will modify the picture. Nevertheless, Fig. 27 clearly reveals that, by approaching the displacive limit, the temperature region where the kink resonance dominates, shrinks to zero. This region expands by approaching the order-disorder regime.

There, the situation becomes rather clear, because in the Ising limit, where

$$\Delta \to \infty, \quad B \to \infty, \quad \text{but } \frac{\Delta}{B} \to 1 \ , \tag{187}$$

the gap of the optic-phonon branch

$$\omega_A^2(0) = -\Delta + 3B\langle y^2\rangle \approx -\Delta + 3B\frac{\Delta}{B} = 2\Delta \tag{188}$$

also tends to infinity. As a consequence, the optic-phonon branch becomes irrelevant, and what remains are kinklike features.[23] In contrast to those in the displacive regime, they will exhibit narrower kink walls. This feature is nicely illustrated in Fig. 27 by the increase of T^* with Δ.

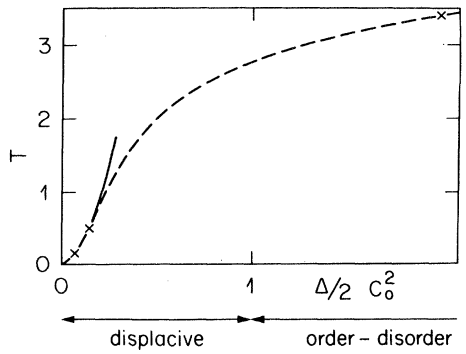

FIG. 27. "Crossover" line [Eq. (182)], where 50% of the spectral weight of $\hat{S}_{yy}(q=0,\omega)$ is in the kink resonance, and 50% in the optic-phonon branch. The crosses mark the MD estimates. For comparison, we included the asymptotic expression resulting from the ideal kink-gas approach [Eq. (185)].

B. $\hat{S}_{y^2y^2}(q,\omega)$

According to the two-phonon approximation, this dynamic form factor is expected to exhibit three resonances for $T \to 0$ [Eq. (94)]. A one-phonon peak, a low-frequency structure steming from the two-phonon difference process and a high-frequency peak due to the sum process around $\omega = 2\omega_{q=0}$. The molecular-dynamics results are shown in Fig. 28 for $k_B T = 0.00448$.

There is a high-frequency peak, close to $\omega_A(q)$ [Eq. (176) and Table XII], corresponding to the one-phonon peak expected, marked by an arrow.

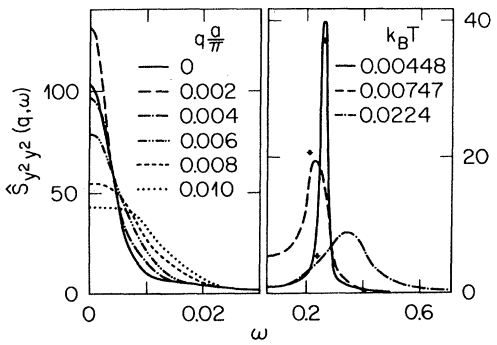

FIG. 28. $\hat{S}_{y^2y^2}(q,\omega)$ for some fixed q values for model III at $k_B T = 0.00448$. The arrows mark the positions $\omega_A(q)$ of the expected one-phonon peak. The high-frequency MD results correspond to $q=0$.

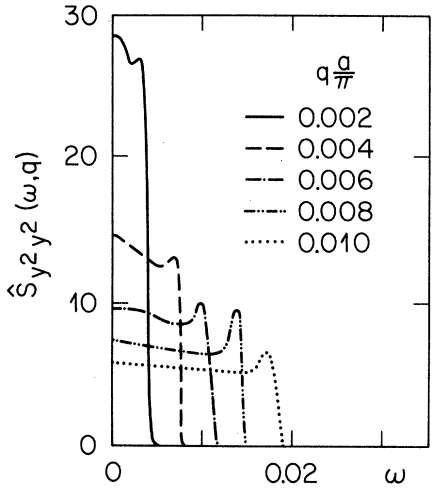

FIG. 29. Two-phonon difference contribution to $\hat{S}_{y^2y^2}(q,\omega)$ [Eq. (94)] for $k_BT=0.00448$ for model III.

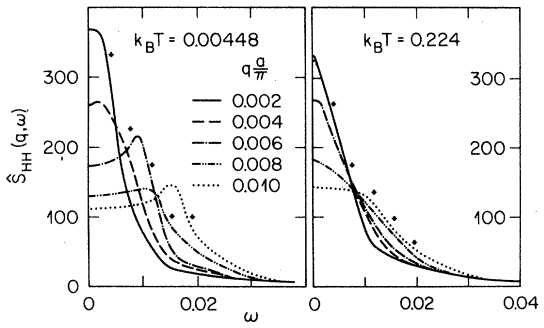

FIG. 30. $\hat{S}_{HH}(q,\omega)$ for some fixed q values for model III. The arrows mark the estimates for the second-sound frequency (Table XII).

The resonance expected from the two-phonon sum process $[\omega\approx 2\omega_A(0)]$ is obviously not resolved. To identify the low-frequency resonance, in Fig. 29 we show the structure resulting from the two-phonon difference process, as obtained from Eq. (94) by numerical evaluation. This contribution is obviously too weak to account for the much stronger low-frequency peaks in Fig. 28. This failure differs from the sG case, where this resonance was rather well reproduced by the two-phonon difference process. In view of this, an unambiguous identification of the low-frequency peak in Fig. 28 is not possible, but it is suggestive that the kink contribution to $S_{y^2y^2}(q,\omega)$ is important in the ϕ^4 system, while in the sG chain, no such evidence became apparent. Another important difference is the strength of the resonance close to $2\omega_A(q=0)$, corresponding to two-phonon sum processes or internal oscillations of breatherlike features. In the sG system, this peak was well resolved (Fig. 16), while in the present case, it is too weak to produce a significant structure in the high-frequency tail of the one-phonon peak (Fig. 28).

C. $\hat{S}_{HH}(q,\omega)$

According to the hydrodynamic approach, this dynamic form factor should exhibit a heat-diffusion or second-sound resonance. Assuming well-defined second sound, its frequency ω_{ss} might be estimated with the aid of Eq. (172). The transfer-integral results are listed in Table XII. MD results for $\hat{S}_{HH}(q,\omega)$ are shown in Fig. 30 for $k_BT=0.00448$. The q dependence of the resonances are obviously consistent with overdamped second sound for $qa/\pi\lesssim 0.004$, becoming underdamped for larger q values. In fact, fully diffusive energy fluctuations are not yet present, because $\hat{S}_{HH}(q,\omega=0)$ is inconsistent with the characteristic q^{-2} dependence of heat diffusion. As seen from Fig. 30, this is also the case at $k_BT=0.224$, so that the crossover from second-sound behavior extends over a rather large temperature interval, even though second sound is less well defined than in the sG chain. For $k_BT\gtrsim 0.00747$, this discrepancy can be understood in terms of the fundamentally different high-temperature behavior. In fact, the sG chain tends to a weakly interacting phonon gas for $T\rightarrow\infty$, while the ϕ^4 chain becomes equivalent to independent quartic oscillators.

ACKNOWLEDGMENTS

We have benefited from illuminating discussions with A. R. Bishop, H. R. Jauslin, J. M. Loveluck, K. Maki, M. Steiner, H. J. Mikeska, and S. E. Trullinger.

[1]T. Schneider and E. Stoll, Phys. Rev. B 22, 5317 (1980).
[2]*Solitons and Condensed-Matter Physics*, edited by A. R. Bishop and T. Schneider (Springer, Berlin, 1978).
[3]S. Aubry, J. Chem. Phys. 64, 3392 (1976).
[4]J. A. Krumhansl and J. R. Schrieffer, Phys. Rev. B 11, 3535 (1975).
[5]G. F. Mazenko and P. S. Sahni, Phys. Rev. B 18, 6139 (1978).
[6]K. Kawasaki, Prog. Theor. Phys. 55, 2029 (1976).
[7]H. J. Mikeska, J. Phys. C 11, L29 (1978).
[8]T. Schneider and E. Stoll, Phys. Rev. Lett. 35, 296 (1975).
[9]T. Schneider and E. Stoll, Phys. Rev. Lett. 41, 1429 (1978).

[10]E. Stoll, T. Schneider, and A. R. Bishop, Phys. Rev. Lett. 42, 937 (1979).
[11]A. C. Scott, F. Y. F. Chu, and D. W. McLaughlin, Proc. IEEE 61, 1443 (1973).
[12]T. Schneider and E. Stoll (unpublished).
[13]H. Mori, Prog. Theor. Phys. 33, 423 (1965); 34, 399 (1965).
[14]T. Schneider and E. Stoll, Phys. Rev. 18, 6468 (1978).
[15]H. Beck, in *Dynamical Properties of Solids,* edited by G. K. Horton and A. A. Maradudin (North-Holland, Amsterdam, 1974), Vol. II, p. 205.
[16]T. Schneider and H. J. Jauslin (unpublished).
[17]J. F. Currie, J. A. Krumhansl, A. R. Bishop, and S. E. Trullinger, Phys. Rev. B 22, 477 (1980).
[18]A. Rahman, Phys. Rev. 136, A405 (1965).
[19]L. Verlet, Phys. Rev. 159, 98 (1967).
[20]T. Schneider and E. Stoll, Phys. Rev. B 17, 1302 (1978).
[21]A. R. Bishop, Solid State Commun. 30, 37 (1979).
[22]M. J. Ablowitz, D. J. Kaup, A. C. Newell, and H. Segur, Phys. Rev. Lett. 30, 1262 (1973).
[23]T. Schneider and E. Stoll, Ferroelectrics 24, 67 (1980).